UNIVERSITY OF CALIFORNIA, SAN DIEGO

A petrological and geochemical study of mantle and crustal xenoliths from Lanzarote, Canary Islands

A Thesis submitted in partial satisfaction of the requirements for the degree Master of Science

in

Earth Sciences

by

Caitlin Mary Traver

Committee in charge:

Professor James M.D. Day, Chair
Professor Geoffrey W. Cook
Professor David R. Hilton

2013

The Thesis of Caitlin Mary Traver is approved, and it is acceptable in quality and form for publication on microfilm and electronically:

Chair

University of California, San Diego

2013

DEDICATION

I would like to dedicate this work to those who have been crucial in my journey to its submission. First I would like to thank the San Diego Foundation (C-2011-00204) and the National Science Foundation (EAR-1116089) for making this project possible through funding for fieldwork, analytical expenses, and summer research financial support. I would like to thank Dave Hilton for his role in getting me hooked on geochemistry as an undergraduate through his enthusiastic and enlightening lectures. I would also like to thank Geoff Cook for sharing his love for geology with every student he has ever had and for being the most supportive professor and friend a person could ask for. I would like to thank James Day for entrusting to me his amazing project on some of the most beautiful and interesting rocks I have ever beheld, and for being the perfect balance of patient and motivational since the project's beginning. I would like to thank my family, especially my parents, for their support and encouragement for my education throughout the years. A lot more instant noodles would have been consumed if they hadn't helped me out, even after I started working as a TA, in the months when the paychecks wouldn't cover the bills. I know I am very lucky indeed to have a family that was willing to help me out so much even when they could barely afford to, and not having a huge pile of student loans to pay off is a relief that will surely make these next years transitioning to a working woman much less scary. I would like to thank all of my lab-mates who have been to many a meeting and cleaned many a lab room by my side. Finally, I have to thank my comrade-in-arms, Jorge Perez. Our friendship began on the lava fields of Hawai'i and continued when we had almost every class together in our final year as undergraduates. If that wasn't enough, we both moved forward to graduate studies in the same lab, under the same advisor, working in the same office for the past year and a half. Although he sometimes drove me crazy and made me want to throw every item in the room at his face, he has become like a brother to me. I am so proud of him now, as we wrap up this last chapter of our studies together, and I am excited to see what he will accomplish in the future; whether it be in research, industry, or education, Jorge, you'll make one hell of a geologist!

TABLE OF CONTENTS

LIST OF FIGURES

LIST OF TABLES

ABSTRACT OF THE THESIS

A petrological and geochemical
study of mantle and crustal xenoliths from
Lanzarote, Canary Islands

by

Caitlin Mary Traver

Master of Science in Earth Sciences

University of California, San Diego, 2013

Professor James M.D. Day, Chair

This study aims to evaluate the processes by which ocean island basalt-derived mantle xenoliths are depleted and, in some cases, subsequently re-fertilized using extremely depleted mantle xenoliths from Lanzarote, Canary Islands. New petrography, mineral-chemistry and whole-rock data are reported for >40 Lanzarote xenoliths, ranging from ultra-depleted harzburgites to re-fertilized lherzolites and gabbroic crustal samples. Previous studies of mantle xenoliths from Lanzarote report

whole rock and mineral chemistries for only general categories of mantle peridotites, *e.g.* dunites, protogranular harzburgites and lherzolites, and melt-influenced textured xenoliths. In these studies, there are few detailed textural and chemical sample-specific connections reported. This study investigates and reports on chemistries and textures of individual samples, as they prove to be intrinsically related. These samples come from a total of six separate sampling sites on Lanzarote, representing one of the most comprehensive petrological studies yet performed on xenoliths from any oceanic island. This study focuses on identifying levels of melt depletion and later melt infiltration into mantle xenoliths and to provide a framework for understanding processes acting on the mantle beneath the Canary Islands.

INTRODUCTION

The mantle plays a fundamental role in the evolution of Earth, acting as a convective engine that drives plate tectonics and as a major control on the terrestrial heat budget (*e.g.*, Turcotte & Schubert, 1982). Lying between the crust and outer core, the mantle is ~2900 km in thickness and constitutes ~84% of Earth's volume. Yet despite the significance of the mantle to terrestrial evolution, our understanding of the compositional variation of this reservoir, which is so critical to understanding of terrestrial geochemical evolution (e.g., Workman & Hart, 2005), is restricted. This is because less dense oceanic and continental crust nearly ubiquitously overlies the mantle with occasional exposure of upper mantle material as mega-mullions and transform-fault and fault-bounded mantle abyssal peridotites on the ocean floor, as continental massif peridotites, obducted ophiolite complexes (Bodinier & Godard, 2003), or as accidentally included mantle xenoliths within predominantly alkaline basalt volcanic rocks (Pearson *et al.,* 2003).

Studies have shown that the upper mantle is predominantly olivine-rich, but that there is likely significant heterogeneity with melt-depleted olivine + orthopyroxene + Cr-spinel harzburgites to initially fertile (essentially not melt-depleted, or very limited melt-depletion) or re-fertilized olivine + orthopyroxene + clinopyroxene + Cr-spinel lherzolite (*e.g.* Simon *et al*., 2008). These rock types are interpreted to reflect primarily fertile mantle or depleted mantle that represent residues after modern to ancient melt extraction. Mantle heterogeneity has important implications for understanding the dynamics of melting in the mantle (*e.g*., Ringwood,

1975), as well as understanding the role of ancient to recent subduction (*e.g.*, Hofmann, 1997; 2003) and mantle differentiation in the early Earth (*e.g.*, Caro *et al.*, 2003; Boyet & Carlson, 2005). A particularly valuable resource for understanding compositional variations in the upper mantle comes from xenoliths included within oceanic island basalts (OIB). Since the oceans span approximately 70% of the Earth's surface, OIB-derived xenoliths allow accidental sampling across this enormous geographic range.

While many studies have been done on continental ultramafic xenoliths (see for example Pearson *et al.*, 2003; Pearson & Wittig, 2008) and ophiolites and orogenic massifs (Bodinier & Godard, 2003) far fewer studies have been conducted on OIB-derived mantle xenoliths. Those studies that were conducted up until 2008 have been reviewed by Simon *et al.* (2008), who reported new and published data for OIB-derived mantle xenoliths from the Atlantic Ocean (Canary Islands, Madeira, the Azores, Cape Verde), Indian Ocean (Kerguelen, Grande Comores) and from the Pacific Ocean (Samoa, Hawaii, and Tahiti). Based on petrography and mineral chemistry, Simon *et al.* (2008) proposed two main classifications for OIB-derived mantle xenoliths of; (1) ultra-refractory mantle material with high whole-rock MgO wt.%, high olivine forsterite (Fo) compositions, high chromian-number (cr#) spinel (cr#= cation ratio Cr/(Cr+Al)), low whole-rock CaO and Al_2O_3 wt.%, and low Al_2O_3 in orthopyroxene (opx) and; (2) fertile to mildly refractory mantle material with lower whole-rock MgO wt.%, lower cr# spinel, higher whole-rock CaO and Al_2O_3 wt.%, and

wider ranges of olivine forsterite compositions. Simon *et al*. (2008) excluded samples that showed textural or evidence for mantle metasomatism and melt interaction because they were considered unrepresentative of upper mantle composition.

Simon *et al.* (2008) showed that many of the islands that they inventoried preserve ultra-refractory mantle xenoliths (Canary Islands, Madeira, Azores, Cape Verde, Kerguelen, Grand Comores, Samoa, Hawaii), but that some islands also contain exclusively (e.g., Tahiti) or occasional (Hawaii, Cape Verde) fertile compositions that presumably reflect lower degrees of melt removal. Simon *et al*. (2008) also demonstrated that ultra-refractory OIB xenoliths were more refractory than abyssal peridotites and have been subjected to higher degrees of partial melting. Simon *et al*. (2008) and Neumann & Simon (2009) have suggested that highly-depleted peridotite is common beneath OIB and, in combination with evidence from Os isotopes in mantle peridotites for long-term and large-scale melt depletion (*e.g*., Widom *et al*., 1999; Coltorti *et al*., 2010), have suggested that it may be a major constituent of the convecting mantle. Finally, Simon *et al*. (2008) demonstrated that, of the refractory OIB-derived xenoliths, those from the Canary Islands represent some of the most extremely depleted, with high whole-rock MgO and low SiO_2 and Al_2O_3.

Here I present a study that is motivated to understand the processes by which OIB-derived mantle xenoliths are depleted – and re-fertilized – using the most extremely depleted mantle xenoliths ever identified, from Lanzarote, Canary Islands. New petrography, mineral-chemistry and whole-rock data are reported for >40

Lanzarote xenoliths, ranging from ultra-depleted harzburgites to re-fertilized lherzolites and gabbroic crustal samples. These samples come from a total of six separate sampling sites on Lanzarote, representing the most comprehensive petrological study yet performed. These samples are also the subject of on-going noble gas (Hilton *et al*., 2008) and Os isotope and highly-siderophile element abundance studies (Day *et al*., 2008) to understand the nature of refractory mantle. This study focuses on identifying levels of melt depletion and later melt infiltration into mantle xenoliths and to provide a framework for understanding processes acting on the mantle beneath the Canary Islands.

GEOLOGICAL SETTING

The Canaries are an age progressive volcanic island chain located ~100 km off the coast of northwest Africa (Figure 1). The Canaries span a lateral distance of ~500 km, trending roughly east–west and are comprised of seven main islands: Lanzarote, Fuerteventura, Gran Canaria, Tenerife, La Gomera, La Palma, and El Hierro. The island chain as a whole has sub-aerial lavas dated from 20.6 million years old to recent historical eruptions (Abdel-Monem *et al*., 1972; Guillou *et al*., 1996; 1998; Paris *et al*., 2005). The westward trending, age-progression of the Canary Islands has been interpreted as symptomatic of a slow-moving mantle 'hotspot' with a low buoyancy flux (Abdel-Monen *et al*., 1972; Morgan, 1981; Malamud & Turcotte, 1999; Carracedo *et al.,* 2001). In addition to both mantle- and crustal-derived xenoliths, the islands host a large range of rock types including alkaline picrites, ankaramites, olivine-phyric and hornblende-bearing basanites and basalts, trachytes, nephelinites, phonolites and carbonatites (Abdel-Monem *et al.,* 1972; Schmincke, 1982; Antigua and Hernan, 2000; Day *et al*. 2010). The Canary Islands lie on some of the oldest oceanic lithosphere in the ocean basins; this lithosphere is Jurassic in age (e.g., Carracedo *et al*., 2002).

Oceanic islands such as the Canaries are formed from magmas derived through decompression melting of either actively or passively upwelling mantle material. The cause of decompression melting is attributed to processes such as anomalously hot mantle rising due to buoyancy or lithospheric cracking (Morgan, 1972; Turcotte &

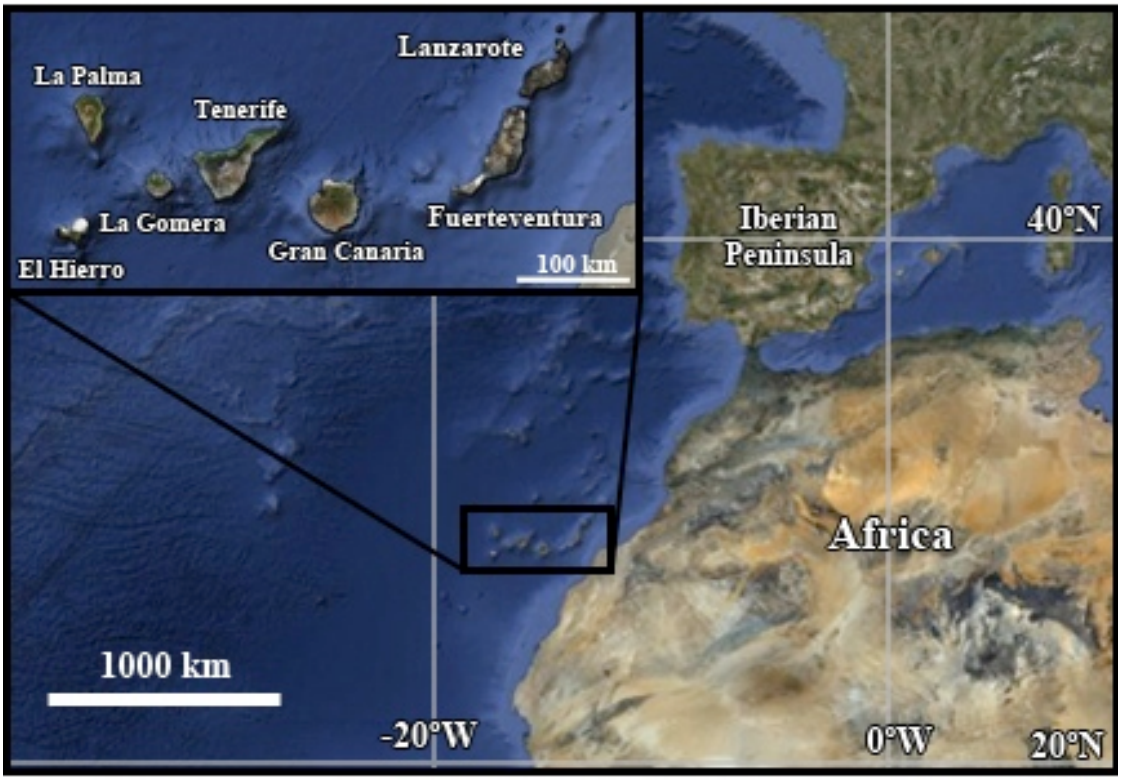

Figure 1: Map of west coast of Africa; Inset of Canary Island Chain (images obtained from Google satellite maps).

Oxburgh, 1976). The cause of partial melting of mantle material and magma generation to form the Canary Islands is debated. One model for the islands' origin is decompression melting due to a propagating fracture (*e.g.* Anguita & Hernan, 1975). In this model, stresses within the plate related to the formation of the Atlas Mountains created sufficient tension to cause fracturing of the lithosphere that propagated away from the continental margin; this can explain the general age progression observed in the Canary Island chain. Carracedo *et al*. (1998) argue that the Canaries conform to a mantle plume origin, attributing the roughness of the age progression to the slow movement of the African plate. Further work proposes a combination of propagating

fracture and mantle plume as the source of decompression melting to form the Canary Islands (*e.g.* Antigua & Hernan, 2000).

The islands follow a general three-stage volcanic history described by Carracedo *et al.* (1998). The first is a large-scale shield-building eruptive stage; the second is represented by a lull in volcanism and deep erosion of the island; the final (post-erosional) stage is a period of active volcanism. Shield-stage volcanism is characterized by fissure eruptions and thick tabular lavas, whereas post erosional gap volcanism is characterized dominantly by cinder cone formation and related lava flows (Antigua & Hernan, 1975). El Hierro, La Palma, and Tenerife are currently in the shield building stage (Carracedo *et al.,* 1998). La Gomera, on the other hand, is in the erosional gap stage and is the only island of the seven without Quaternary volcanism (Carracedo *et al.,* 1998). The remaining islands, Gran Canaria, Fuerteventura, and Lanzarote, are considered to be in the post-erosional volcanism stage (Carracedo *et al.,* 1998). Many of the xenolith localities in the Canary Islands occur within Holocene to recent volcanic units that either relate to post-erosional volcanism (Lanzarote, Fuerteventura), or alkali basalts from the main shield-stage (El Hierro, La Palma, La Gomera, Tenerife).

Lanzarote is the easternmost and northernmost of the seven main islands. Two shield complexes make up the bulk of the island—the Fumara massif in the north and the Ajache massif in the south. The Fumara massif lavas have been dated between 6 and 12 Ma, and the Ajache massif lavas are dated between 6 and 8 Ma (Abdel-Monem *et al*., 1972). In addition to the shield material, Lanzarote also has post-erosional

eruptive material characterized by smaller-scale flow units and pyroclastic cones (Marinoni and Pasquare, 1994). Most of the exposed rock on Lanzarote is Quaternary in age, including the products of the historical eruption lasting from 1730-1736, during which time material was erupted from more than 30 vents in the western-central part of the island (Carracedo *et al*., 1992; Carracedo & Day, 2002).

Mantle (and some crustal) xenoliths occur on the islands of Lanzarote, Fuerteventura, Tenerife, La Gomera, El Hierro and La Palma and petrological and fluid-inclusion studies have previously been performed on xenoliths found at localities within these islands (Neumann, 1991; Siena *et al*., 1991; Frezotti *et al*., 1994; 2002a,b; Neumann *et al*., 1995; 2002; 2004; Wulff-Pedersen *et al*., 1996; Abu Al-Rus *et al*., 2006; Simon *et al*., 2008). Of these studies, only Neumann *et al*. (1995) and Siena *et al*. (1991) have considered the petrology of Lanzarote mantle xenoliths in any detail. Both studies reported on harzburgites, rare lherzolites, and spinel dunites from Quaternary age eruptive material from Series III and IV of Fuster *et al*. (1968) finding that the mantle reservoir beneath Lanzarote is best represented by highly deformed refractory harzburgites and dunites that are on average more refractory than abyssal peridotites.

METHODS

Sampling

A suite of xenoliths collected from six separate localities on the island of Lanzarote were studied. These xenoliths were found exclusively within post-erosional volcanic stage eruptive material from Quaternary age cones or maars (Series III and IV lavas of Fuster *et al*., 1968), affording east-west coverage of the island (Figure 2). Some of these cones were formed during the 1730-1736 historical eruption: Caldera de Los Cuervos, Pico Partido, and Montaña de Las Nueces localities (e.g., Carracedo *et al*., 1992). El Golfo Maar, Guatiza cones, and El Cuchillo Maar localities were formed earlier as Quaternary-aged volcanic formations. Xenoliths were sampled directly from where they were originally emplaced in eruptive material, or where weathered out of eruptive material and still proximal to their volcanic source.

General hand sample descriptions and GPS locations for all samples are shown in Table A1. Some sampling biases were unavoidable. Size was a consideration; xenoliths had to be large enough to execute all planned analyses. Another limitation was location; in heavily trafficked tourist areas, like El Golfo Maar, minimal sampling could be done. Also sampling could only be done outside the boundaries of Timanfaya National Park which covers ~50 km^2, about one fourth of the area of the 1730-1736 eruption. Direct observation from a tour of Montañas del Fuego in Timanfaya proved that ultramafic xenoliths are present in at least some of these cones. In the maar localities, El Cuchillo and El Golfo, most xenoliths observed in the field were not more than 10 cm across and were typically much smaller than 10 cm across. In cinder

cone localities, xenoliths were observed that were as large as 25 cm across. This discrepancy in size distribution is due to the fact that the formation of a maar is a considerably more explosive process than the formation of a cinder cone. See Figures 3 and 4 for examples of field locations and field photographs of xenoliths. Eight xenolith samples from the 2006 collection campaign by Day and Hilton, thirty-five from the 2010 field campaign by Day, and twenty-seven from the 2012 field campaign by Traver and Day for a total of seventy Lanzarote crustal and mantle xenoliths.

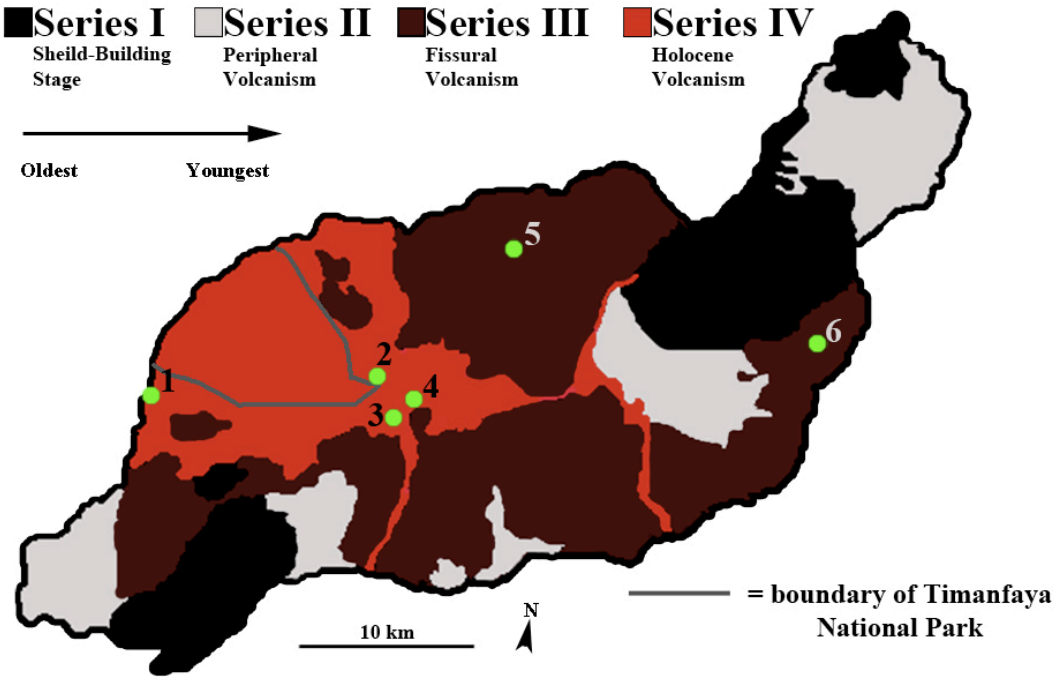

Figure 2: Modified from Neumann *et al*., 1995 Figure 1, Series I-IV as defined by Fuster *et al*. (1968); Localities: 1) El Golfo Maar 2) Pico Partido 3) Caldera de Los Cuervos 4) Montana de Las Nueces 5) El Cuchillo Maar 6) Guatiza; Exact GPS locations are listed in Table A1.

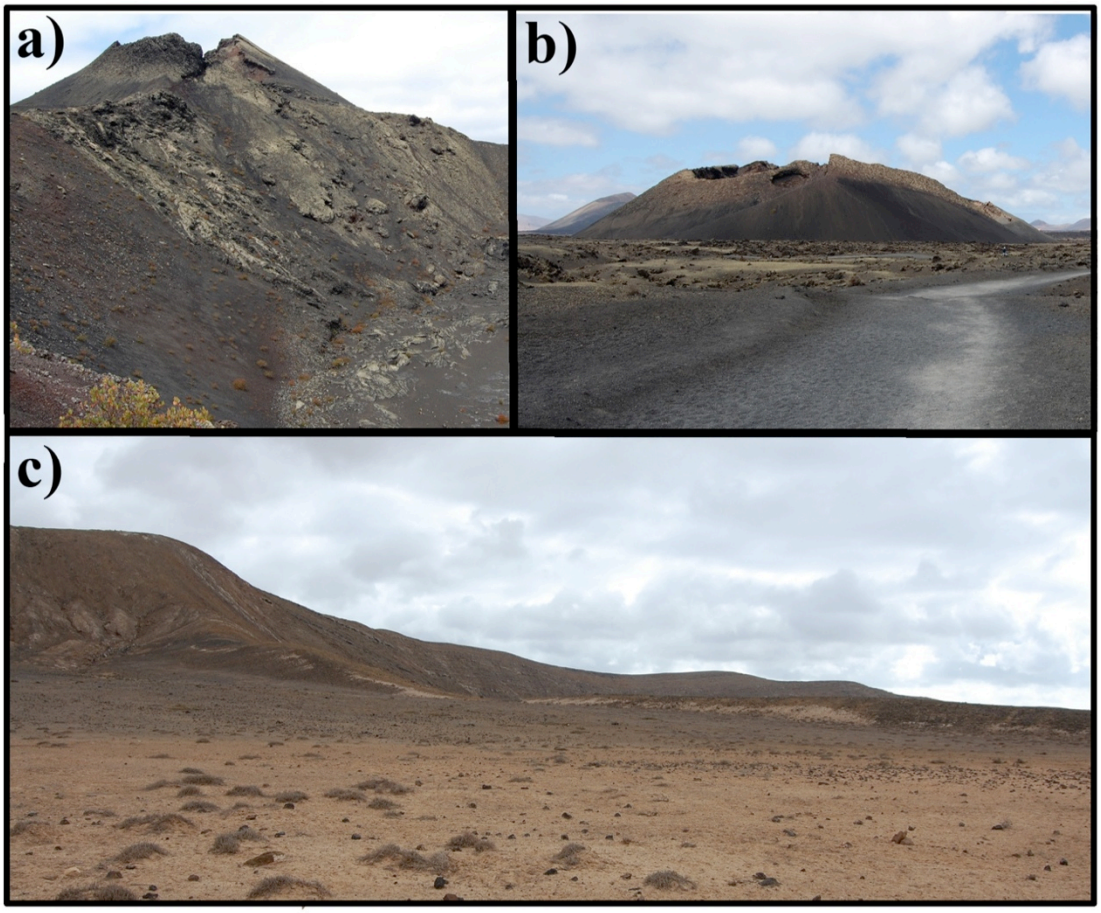

Figure 3: Examples of xenolith localities; **a)** Pico Partido (cone), highest point of Pico Partido is approximately 100 m above photograph site **b)** Caldera de Los Cuervos (cone); from this perspective, cone is approximately 275 m wide **c)** El Cuchillo Maar, from ridge in foreground to opposite side of the maar is approximately 1 km; ridge in foreground is approximately 100 m above photograph site. Images were taken during the 2012 xenolith collection campaign.

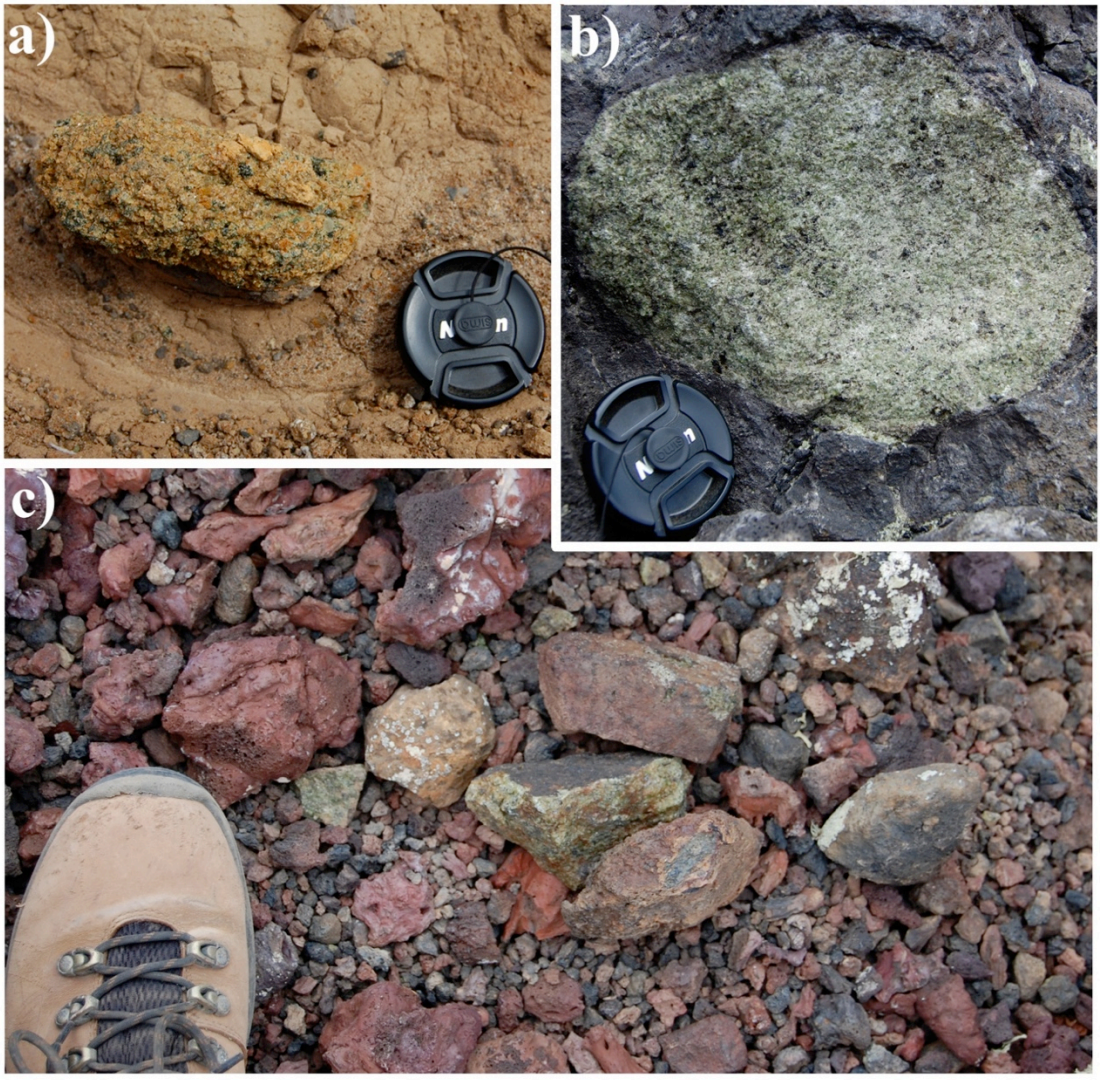

Figure 4: Field photographs of xenoliths; **a)** Lherzolite at El Cuchillo Maar, bomb sag caused by xenolith visible **b)** Large harzburgite embedded in lava at Caldera de Los Cuervos **c)** Multiple loose xenoliths atop Pico Partido; Scale of Nikon cap is 55 mm diameter.

Petrography

For the xenolith samples analyzed for this study, billets were cut targeting the xenolith component. These billets were then made into thin sections by San Diego Petrographics. Petrographic observations made for samples under polarized and cross-polarized transmitted light include the following: overall textures, presence and extent of secondary grains, presence of melt infiltration, descriptions of the appearance and

size of mineral phases present. Modal mineralogy was determined using a film scanner and ImageJ program using a new method developed here. Briefly, by scanning in a polarized image of each thin section, isolating an area entirely covered by sample, converting to gray-scale, and carefully choosing thresholds for all mineral phases present, a quantitative modal mineralogy was established. The detailed instructions for this process using the equipment in the Scripps Isotope Geochemistry Laboratory (SIGL) are included in the Appendix.

Mineral Chemistry

Minerals were separated from an aliquant of crushed material for electron micro-probe (EMP) analysis. Grains of all mineral phases present were separated from the crushed material of each sample. Mineral phases separated include olivine, orthopyroxene, spinel, clinopyroxene, and plagioclase. Mounts of selected grains were made then taken to the University of California, Santa Barbara for analysis using the Cameca SX-100 electron microprobe of the Earth Sciences Electron Microscopy, Diffraction and Micro-Analysis Laboratory. Mineral compositions were determined in wave-length dispersive spectral mode using an accelerating potential of 15 keV, a 10-15 nA beam current, with beam focus of 1 μm. Peak and background counting times of 20 s and standard ZAF (PAP) correction procedures were used. Plagioclase compositions were determined using a 10 nA beam current, a 5 μm beam size, and longer counting times to avoid mobilization of Na or K. Natural and synthetic standards were used for calibration. Drift was within counting error through the

analytical session. Detection limits (3σ above background) were <0.03 wt.% for all elements listed.

Textural and elemental relationships of four thin sections were investigated using the Scanning Electron Microscope at the Calit2 Nano3 facility at the University of California, San Diego. The microscope used was a Philips XL30 field-emission Environmental Scanning Electron Microscope equipped with an Oxford Link Pentafet detector with a 10 mm^2 window. The microscope was used to perform Energy Dispersive X-ray Spectrometry with a beam energy of 20 kV at a working distance of 10 mm and an average of ~5000 x-ray counts per second. Elemental standards used were obtained from the University of Oxford.

Whole-rock geochemistry

At least half of each xenolith sample was set aside for preservation and future study. The rest of the material was coned-and-quartered and prepared for whole-rock powders or for coarse crush for mineral separation (see above). After making billets for thin sections, remaining material was sawn and subsequently processed using a ceramic plate crusher. At least 11 grams of crush material from each sample, up to 80 g for xenoliths with the most available material, was then powdered using a ceramic shatter box. Finely ground powders of each sample were packaged and shipped to the X-ray Laboratory of Franklin and Marshal College for major and trace element analyses using a PW2404 Panalytical, Inc. XRF vacuum spectrometer. Major elements were measured by using lithium tetraborate flux and whole rock powder fused into

glass discs, which were then used for X-ray fluorescence (XRF) analysis. For trace element analyses, whole-rock powder was combined with high purity Copolywax powder to make briquettes, which were then used for XRF trace-element determinations. Working curves for all major and trace elements were determined by analyzing geochemical rock standards. For major elements, all the errors that could accrue from weighing, mixing, preparation of the fusion glass disk, and peak and background measurements yield an uncertainty of <0.1 wt.% (0.02 wt.% for Na_2O, and 0.005 wt.% for Al_2O_3, which are the lowest whole rock-constituent oxides critically discussed for the purposes of this study). For trace elements discussed in this study, all the errors that could accrue from preparation and instrumentation yield an uncertainty of <5% from the accepted value for geochemical standards with the exception of Ba, having >10% variation from the accepted standard value.

RESULTS

For this study, 43 xenoliths from the 2006 and 2010 field campaigns (LZ06* and LZ10* samples) were analyzed. Of these, twenty-eight were classified as harzburgites, three as lherzolites, five as dunites and seven as crustal xenoliths. These classifications are based on petrography and are in agreement with geochemical results. Xenoliths are angular to sub-rounded and vary in size from ~5 to 15+ cm across; see Table A1 for hand sample descriptions.

Petrography

See Table 1 for a summary of sample-specific petrography and Table 2 for modal mineralogy. Harzburgite, lherzolite, and dunite samples are plotted on the ultramafic ternary diagram in Figure 7. Fractures were observed in most peridotite samples; fractures are sometimes unfilled and others are filled mostly with small amounts of basaltic glass. Some xenoliths display both filled and unfilled fractures.

Harzburgites

Harzburgites are dominantly protogranular to porphyroclastic. Protogranular textures are defined by clean grain boundaries, pristine primary grains and lack of melt infiltration. Porphyroclastic textures are defined by degraded primary grains of pyroxene and sometimes olivine. Degraded orthopyroxenes contain small recrystallized clinopyroxenes throughout the opx grains. Melt infiltration is represented by basaltic glass that is brown in plane polarized light and is present in

many samples with porphyroclastic textures. Olivine composes 50-80 vol.% of the harzburgite samples. The majority of the olivine grains present in the peridotite xenoliths are highly fractured and display kink-bands (Figure 5e). Olivine, the dominant phase in these samples, typically also represents the largest of the primary grains, sometimes measuring up to 15 mm. Olivines are typically not degraded, but can be in the most degraded samples, though always to a lesser extent than pyroxene. Pyroxene represents 18-43 vol.% of harzburgite samples, orthopyroxene (opx) representing 17-40 vol.% and clinopyroxene (cpx) representing trace to 4 vol.% of primary grains. Many pyroxene grains are highly exsolved. In protogranular xenoliths, exsolution lamellae are absent in the rims of opx and cpx grains. Pyroxenes in porphyroclastic samples display varying extents of degradation. High calcium cpx (diopside as opposed to pigeonite and augite) is rarely found as primary grains. Spinel (spl) represents 0.1-2.6 vol.% of harzburgite samples. In protogranular xenoliths, spinels occur as large irregular to rounded grains, as large as 3 mm in some samples, and are most commonly associated with pyroxenes, especially clinopyroxenes if present. In porphyroclastic xenoliths, spinel is also found as fine-grained rounded to polygonal grains in with fine-grained secondary of opx + cpx. Spinel color varies from light brown or reddish brown to dark brown/black in plane transmitted light. In many protogranular samples, spinel and orthopyroxene occur with symplectic texture. A similar relationship between spinel and pyroxene occurs in porphyroclastic samples but with fine-grained recrystallized opx and cpx instead of primary pyroxenes (Figure 5a,b). Occasionally trace amounts of phlogopite are found within fractures. In some

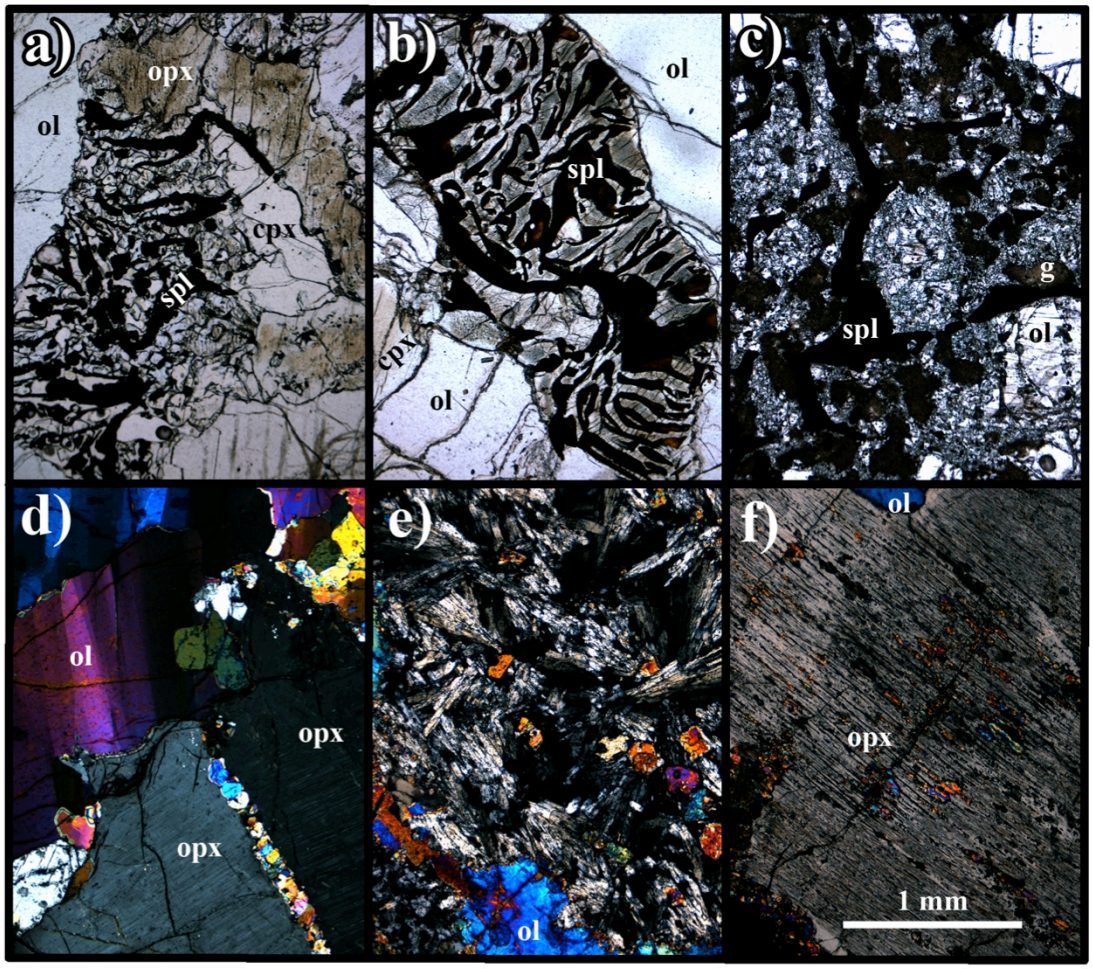

Figure 5: Harzburgite samples showing **a)** Symplectic spinel (spl) and secondary pyroxene grains in sample LZ0604C; plane polarized light (ppl) **b)** Symplectic spinel and primary orthopyroxene (opx) and clinopyroxene (cpx) grains in sample LZ0604C; ppl **c)** Spinel grains, basaltic glass (g), and secondary (sec) grains in sample LZ0602A; ppl **d)** Photomicrograph of sample LZ1017A showing kink-banded olivine, exsolved opx, and a secondary vein; cross polarized light (xpl) **e)** Region of opx rich secondary zone in LZ1016I; xpl **f)** Example of highly degraded orthopyroxene in sample LZ1007; xpl. Scale applies to all 6 photomicrographs.

samples (LZ1003A, LZ1016B, LZ1016I), secondary grains of opx + ol ± cpx have entirely replaced almost all pyroxene grains throughout the sections (Figure 5e). The primary olivines within these samples are highly degraded. Olivines in sample LZ1016B are also highly strained and elongated. The large orthopyroxene porphyroclasts that are rarely found within these sections are highly degraded. Large (>1mm) spinels are present in all three of these samples. Spinel is also present in the

secondary phases. The secondary phases occupy 30-50 vol.%, and are dominantly opx.

Lherzolites

Three of the peridotite samples were found to have >5 vol.% cpx, from 6 to 25 vol.%, defining them as lherzolites. All three lherzolite samples were collected from El Cuchillo Maar. The sample with the highest cpx content, LZ1014, has a vein dominated by cpx as well as fine secondary grains and basaltic glass that cuts across the whole xenolith (Figure 6a) and can be seen in hand-sample (Figure 7). Sample LZ1012A (~6 vol.% cpx) is a protogranular lherzolite, which has an overall finer-grained primary texture than most other peridotite samples (Figure 6c). LZ1008 is a lherzolite with melt infiltration and fine-grained secondary phases of cpx + opx + spl concentrated around large primary spinel grains (Figure 6b). Primary cpx and opx (19-30 vol.%) were both present in these samples, with cpx grains typically being larger than opx grains. Primary olivines are similar to those of the harzburgite group. Large, primary spinels in lherzolite samples are brown to black in ppl and are spatially associated with pyroxenes. Spinels represent from 0.33 to 0.64 vol.% of in lherzolite samples and have similar sizes and relationships to those of the harzburgite group.

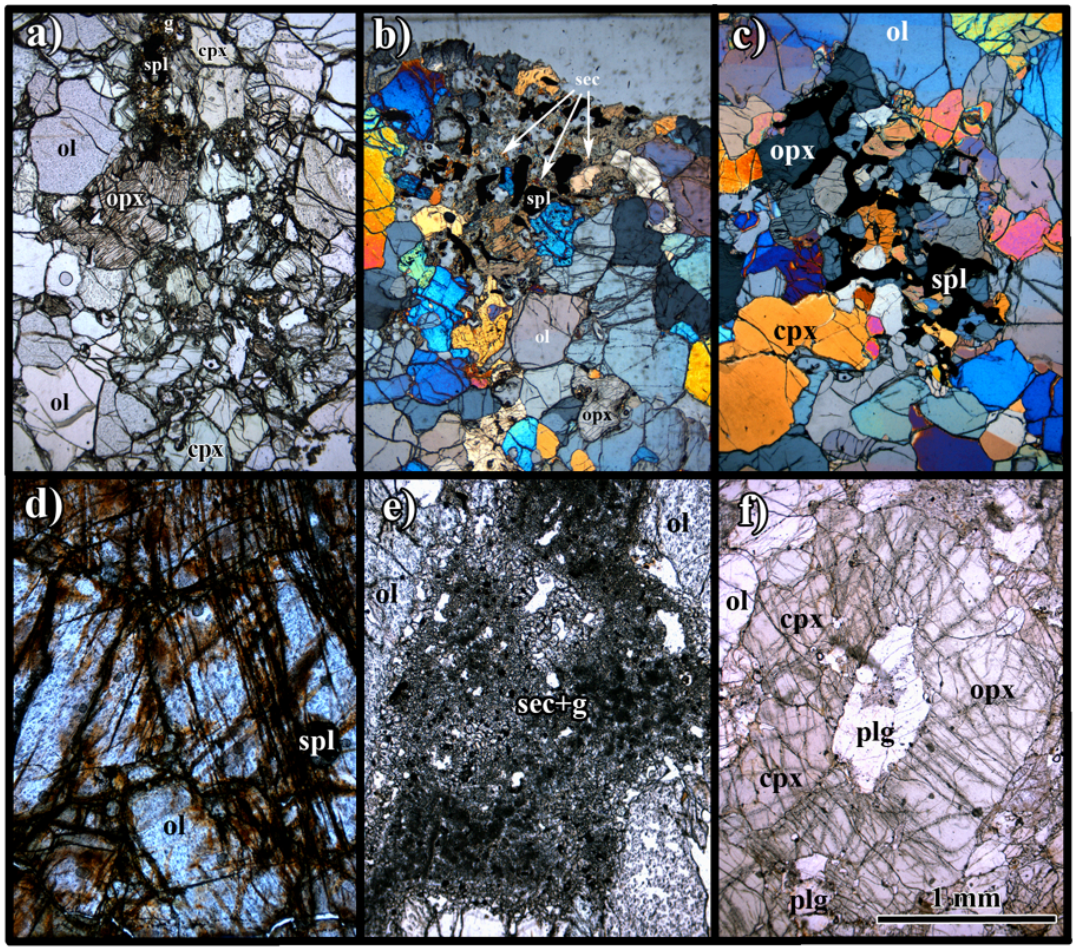

Figure 6: a) Photomicrograph dominated by cpx vein described in text, lherzolite LZ1014; xpl **b)** Secondary grains surrounding spinel in LZ1008, a lherzolite; xpl **c)** Protogranular lherzolite LZ1012A, cpx grains are dominantly pigeonite-augite in this sample; xpl **d)** oxidation of olivine in dunite sample LZ1016D; ppl **e)** Melt infiltration in dunite sample LZ1016E, indicated by the presence of extensive secondary grains and basaltic glass; ppl **f)** Photomicrograph of olivine gabbro sample LZ1016C; ppl. Scale applies to all 6 photomicrographs.

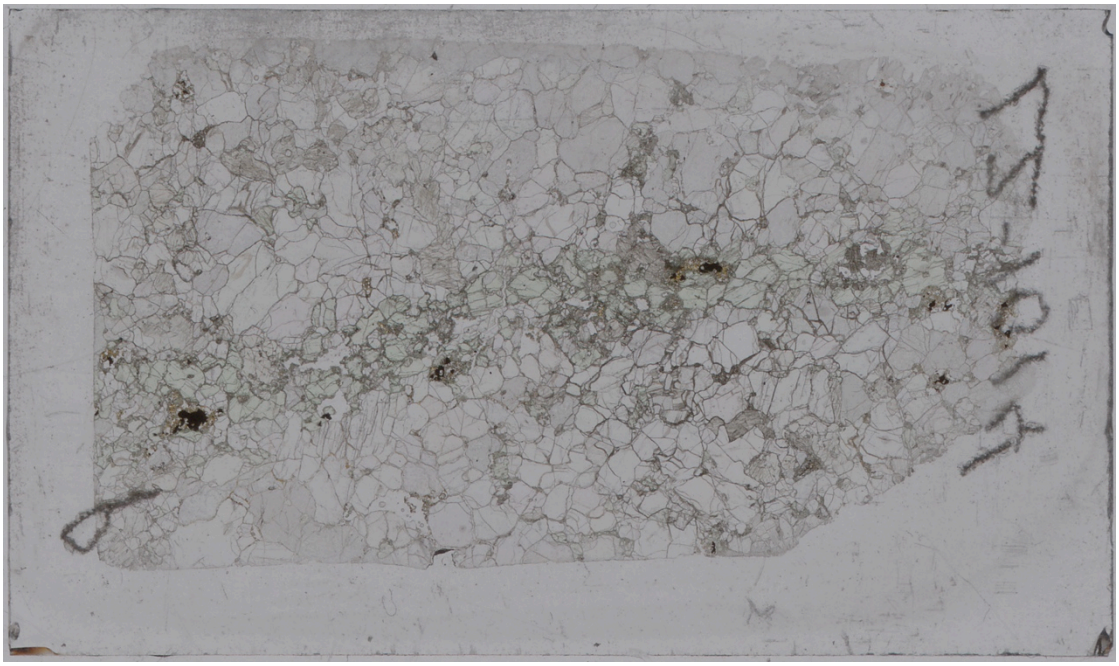

Figure 7: Lherzolite LZ1014, full slide in ppl; cpx (green) vein cuts across xenolith; spinel (black) enclosed in basaltic glass and secondary grains found within cpx vein; slide mount is 2.1 x 3.6 cm.

Dunites

Dunite samples collected were from Guatiza cones. The dunite samples contain little to no primary pyroxene grains. Sample LZ1016Hii contained rare low Ca cpx grains. Dunites consistently have large (>1mm) spinels distributed throughout, between 1-3 vol.% spinel. Spinels are generally irregular to rounded. Some dunites contained infiltrated basaltic glass. Sample LZ1016E has extensive secondary grains and melt infiltration (Figure 6e). Many of the dunites were highly oxidized, exhibiting iddingsitized olivines especially along grain boundaries and cracks (Figure 6d). Olivines in two dunites (LZ1016E, LZ1016Gii) show kink banding, while it is not present in the other samples. Olivine grain size has a narrow range in some dunites, but varies widely in others from 1 to 8 mm.

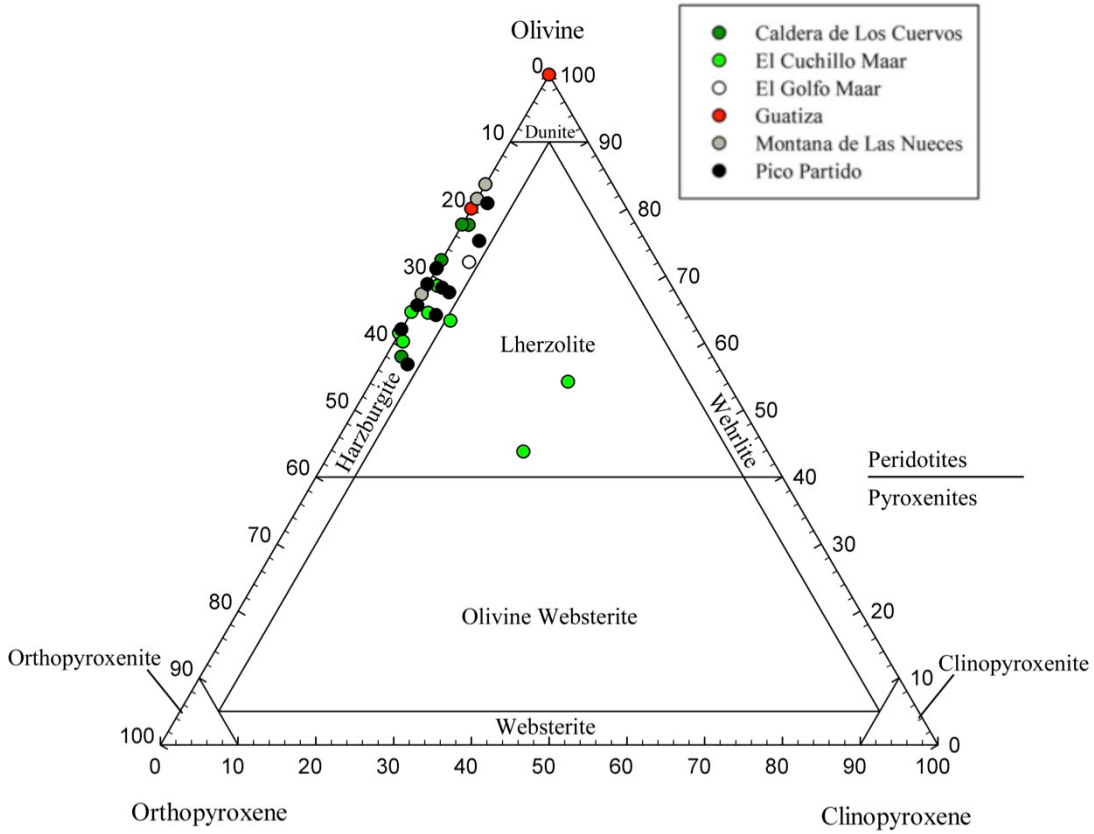

Figure 8: Ternary of mantle peridotites of this study, modal proportions calculated using the ImageJ protocol outlined in methods.

Crustal Xenoliths

The seven crustal xenolith samples contained dominantly plagioclase and clinopyroxene and sometimes significant proportions of olivine. Five of these are gabbros; LZ1013A, LZ1015Aii, LZ1015B, LZ116A, and LZ1016Gi. Gabbro LZ1013A is from El-Cuchillo Maar, all other crustal xenoliths are from Guatiza cones. Pyroxene represents between 48 and 63 vol.% of gabbro samples; this is dominantly clinopyroxene for all samples, only trace amounts of orthopyroxene were observed in samples LZ1016A and LZ1015Aii. Pyroxenes in these gabbros are often sub-rounded. Olivines present were typically iddingsitized and represent from 0 to 2 vol.%.

Plagioclase represents 37-59 vol.% in gabbro samples. Gabbros LZ1013A, LZ1015B, and LZ1016A have similar textures and modal percentages. Pyroxene in these three gabbros are typically 5 to 8 mm, plagioclases are slightly smaller, 2 to 5 mm. LZ1015B has significantly more basaltic glass infiltration than other gabbros. LZ1015Aii has the largest vol.% olivines (iddingsitized) of all the gabbros, and has a much smaller overall-grain size, most grains being ~2 mm across. LZ1016Gii exhibits recrystallized pyroxenes and plagioclases, while retaining original textural relationships.

One crustal xenolith was particularly rich in olivine, and is classified, based on its modal mineralogy, as a plagioclase-bearing lherzolite (~1 vol.% plagioclase) (Figure 6f). The presence of plagioclase, lack of spinel, and observed textures indicate that this represents a low pressure cumulate and is therefore grouped with other crustal xenoliths. Sample LZ1015Ai contains olivine and plagioclase. Plagioclase represents ~60 vol.% and has the largest grain sizes in this sample. Modal mineralogy places this as the cumulate rock type troctolite. Sample LZ1015Ai also has multiple veins of melt infiltration that collectively cover over 20 vol.% of the section.

Table 1: Petrography data

Specimen	Rock Type	Melt[1]	Comments	Mineral Phases[2]
LZ1001A	Harzburgite	basaltic glass, degraded pyroxenes		Ol, Opx, Spl, Sec, G
LZ1001B	Harzburgite	basaltic glass, degraded pyroxenes		Ol, Opx, Spl, Sec, G
LZ1002	Harzburgite	small amount basaltic glass, some px degraded	poikilitic ol in opx	Ol, Opx, Spl, Sec, G
LZ1003A	Harzburgite	pyroxenes recrystallized	no primary pyroxene, relict texture, replaced by secondary	Ol, Sec
LZ1003B	Harzburgite	none	small vol% low calcium cpx	Ol, Opx, Cpx, Spl
LZ1003C	Harzburgite	none	small vol% low calcium cpx	Ol, Opx, Cpx, Spl
LZ1004A	Harzburgite	basaltic glass, pyroxene degraded	melt infiltration	Ol, Opx, Spl, Plag, Sec, G
LZ1004B	Harzburgite	degraded pyroxenes	small vol% low calcium cpx	Ol, Opx, Cpx, Spl, Sec
LZ1005	Harzburgite	basaltic glass, degraded pyroxenes	small vol% low calcium cpx	Ol, Opx, Cpx, Spl, Sec, G
LZ1006	Harzburgite	basaltic glass, degraded pyroxenes	small vol% low calcium cpx	Ol, Opx, Cpx, Spl, Sec, G
LZ1007	Harzburgite	basaltic glass, degraded pyroxenes	small vol% low calcium cpx; large range of olivine grain sizes, 1-10mm	Ol, Opx, Cpx, Spl, Sec, G
LZ1008	Lherzolite	basaltic glass, some px degraded	primary cpx (diopside), transition of grain size across slide	Ol, Opx, Cpx, Spl, Sec, G
LZ1009	Harzburgite	basaltic glass, degraded pyroxenes	olivines oxidized	Ol, Opx, Spl, Sec, G
LZ10010	Harzburgite	basaltic glass, degraded pyroxenes	small vol% low calcium cpx	Ol, Opx,Cpx, Spl, Sec, G
LZ1011	Harzburgite	basaltic glass, degraded pyroxenes		Ol, Opx, Spl, Sec, G
LZ1012A	Lherzolite	none	low calcium cpx and diopside present	Ol, Opx, Cpx, Spl
LZ1012B	Harzburgite	some pyroxenes degraded	small vol% low calcium cpx; veins cutting primary grains; highly strained olivines; oxidized	Ol, Opx, Spl, Sec
LZ1013A	Gabbro	none		Plag, Cpx, Opx
LZ1014	Lherzolite	basaltic glass, degraded pyroxenes	cpx (diopside) and Secblast dominated vein accros xenolith	Ol, Opx, Cpx, Spl, Sec, G
LZ1015Ai	Troctolite	none	crossing subparallel veins of secondary throughout slide	Plag, Cpx, Ol, Sec
LZ1015Aii	Gabbro	none	olivines highly altered to iddingsite	Plag, Cpx, Ol
LZ1015B	Gabbro	none		Plag, Cpx

[1] Evidence of melt infiltration and/or melt interacion

[2] Ol=olivine, Opx=orthopyroxene, Cpx=clinopyroxene, Spl=spinel, Sec=secondary grains, Plag=plagioclase, G=basaltic glass

Table 1: Continued

Specimen	Rock Type	Melt[1]	Comments	Mineral Phases[2]
LZ1016A	Gabbro	none		Plag, Cpx
LZ1016B	Harzburgite	pyroxenes recrystallized	no primary pyroxene, relict texture, replaced by secondary; spinels red-brown in ppl	Ol, Spl, Sec
LZ1016C	Plag-Lherzolite	none	significant modal percent olivines	Ol, Plag, Cpx, Opx
LZ1016D	Dunite	none	all olivines oxidized	Ol, Spl
LZ1016E	Dunite	basaltic glass	melt infiltration	Ol, Spl, Sec, G
LZ1016F	Harzburgite	none	small vol% low calcium cpx	Ol, Opx, Cpx, Spl, Sec
LZ1016Gi	Gabbro	none		Plag, Cpx, Ol
LZ1016Gii	Dunite	small amount baslatic glass in cracks	spinels very dark in ppl, rounded; highly strained olivines; olivines oxidized	Ol, Spl, Sec, G
LZ1016Hi	Dunite	none	spinels medium brown in ppl, angular	Ol, Spl
LZ1016Hii	Dunite	basaltic glass	spinels very dark in ppl, rounded; melt infiltration*	Ol, Spl, Plag, Sec, G
LZ1016I	Harzburgite	pyroxenes recrystalyzed	no primary pyroxene, relict texture, replaced by secondary; highly strained olivines; olivines degraded	Ol, Spl, Sec
LZ1017A	Harzburgite	none	large, highly strained olivines; poikilitic opx in ol	Ol, Opx, Spl, Sec
LZ1017B	Harzburgite	none	highly strained, elongate olivines	Ol, Opx, Spl, Sec
LZ0602A	Harzburgite	basaltic glass, degraded pyroxenes		Ol, Opx, Spl, Sec, G
LZ0602B	Harzburgite	basaltic glass, degraded pyroxenes	large secondary dominated zones (7mm and 12mm)	Ol, Opx, Spl, Sec, G
LZ0603i	Harzburgite	(glass limited to near xenolith-host boundary)	small vol% low calcium cpx	Ol, Opx, Cpx, Spl
LZ0604A	Harzburgite	none	small vol% low calcium cpx. Diopside present.	Ol, Opx, Cpx, Spl, Sec
LZ0604B	Harzburgite	none	very large olivines	Ol, Opx, Spl, Sec
LZ0604C	Harzburgite	pyroxenes degraded	large olivines	Ol, Opx, Spl, Sec
LZ0604D	Harzburgite	none	small vol% low calcium cpx; poikilitic ol in opx, several large olivines, most small	Ol, Opx, Cpx, Spl, Sec
LZ0605	Harzburgite	pyroxenes degraded	olivines degraded	Ol, Opx, Spl, Sec

[1] Evidence of melt infiltration and/or melt interacion

[2] Ol=olivine, Opx=orthopyroxene, Cpx=clinopyroxene, Spl=spinel, Sec=secondary grains, Plag=plagioclase, G=basaltic glass

Table 2: Modal percentages

Sample	ol	opx	cpx	px (total)[1]	spl	melt+sec	plag
LZ0602A	69.8	28.5	-	-	0.1	1.8	-
LZ0602B	74.6	20.7	0.8	-	1.3	2.5	-
LZ0603i	54.6	37.8	1.9	-	2.6	2.7	-
LZ0604A	56.1	39.4	3.4	-	0.7	0.5	-
LZ0604B	70.8	28.8	-	-	0.1	0.2	-
LZ0604C	68.0	30.9	-	-	0.2	0.9	-
LZ0604D	67.2	29.2	2.1	-	1.4	0.0	-
LZ0605	74.6	24.2	-	-	0.2	1.1	-
LZ1001A	76.3	22.0	-	-	0.6	1.2	-
LZ1001B	71.5	27.4	-	-	0.8	0.3	-
LZ1002	65.1	33.9	0.3	-	0.3	0.4	-
LZ1003A	50.7	-	-	-	0.6	48.7	-
LZ1003B	63.2	32.0	3.4	-	1.4	0.0	-
LZ1003C	74.3	21.2	3.4	-	1.2	0.0	-
LZ1004A	58.0	35.6	-	-	0.3	6.2	-
LZ1004B	66.6	28.7	3.4	-	0.4	0.8	-
LZ1005	80.2	17.4	1.7	-	0.5	0.3	-
LZ1006	70.8	23.9	3.6	-	0.2	1.5	-
LZ1007	67.3	29.6	1.4	-	0.2	1.6	-
LZ1008	41.7	30.0	23.7	-	0.4	4.3	-
LZ1009	57.6	36.2	-	-	0.3	5.9	-
LZ1010	60.6	31.3	2.1	-	0.7	5.3	-
LZ1011	60.3	27.5	-	-	0.2	12.1	-
LZ1012A	62.9	30.8	5.6	-	0.6	0.0	-
LZ1012B	54.8	35.3	1.0	-	0.5	8.4	-
LZ1013A	-	-	-	48.0	0.1	0.0	51.9
LZ1014	51.3	19.4	24.0	-	0.3	5.0	-
LZ1015Ai	-	-	-	19.5	-	22.0	58.5
LZ1015Aii	1.9	-	-	61.9	-	0.0	36.2
LZ1015B	-	-	-	50.8	-	0.0	49.2
LZ1016A	-	-	-	62.6	-	0.0	37.4
LZ1016B	70.0	-	-	-	1.8	28.2	-
LZ1016C	48.2	-	-	50.9	-	0.0	1.0
LZ1016D	98.5	-	-	-	1.5	0.0	-
LZ1016E	61.9	-	-	-	1.6	36.5	-
LZ1016F	(80)	-	(20)	-	(<1)	-	-
LZ1016Gi	-	-	-	49.8	-	0.0	50.2
LZ1016Gii	94.4	-	-	-	3.0	2.6	-
LZ1016Hi	98.0	-	-	-	2.0	0.0	-
LZ1016Hii	95.6	-	-	-	1.3	3.1	-
LZ1016I	52.8	-	-	-	0.4	46.8	-
LZ1017A	80.5	18.3	-	-	0.1	1.0	-
LZ1017B	66.1	32.2	-	-	0.2	1.6	-

[1] For gabbros, total pyroxene measured

[2] Sample LZ1016F modal percentages estimated, polishing roughness no suitable for ImageJ program

SEM

Scanning electron microscopy (SEM) was used for imaging and creating elemental maps of selected zones in thin sections of four of the samples: LZ0602B, LZ1014, LZ1016B, and LZ1016E. This allowed for an understanding of *in situ* major element relationships beyond what could be understood from petrography alone.

In lherzolite sample LZ1014, Element Dispersive Spectrometry (EDS) maps show that secondary grains are typically richer in calcium than in magnesium and iron. This, paired with petrographic observation, allows for the determination of clinopyroxene as the dominant phase of the secondary grains in this sample. Sample LZ1014 has a cpx and fine-grained secondary vein cutting the sample. Orthopyroxene near the cpx rich vein shows no perceivable enrichment of Ca near the rims or depletion away from the vein. Ti and K enrichments observed are the result of melt infiltration.

EDS maps for regions of sample LZ1016B (having approximately 70% olivine porphyroclasts and 30% secondary grains) show that the secondary grains are not enriched in Ca, but are Mg and, to a lesser extent, Fe silicates. SEM data and petrographic data show that secondary grains in this sample are orthopyroxene and olivine, plus spinel. This sample and the other two in its petrographic category fall in with the other harzburgites on all major element plots.

Sample LZ1016E is a dunite with extensive secondary grains. EDS maps of secondary rich regions of this sample are rich in Mg, Ca and Al silicates and contain very little Fe. No primary pyroxenes were observed in thin section, but EDS maps

show that the secondary grains are opx and cpx and relict textures suggest that primary pyroxenes were present in the protolith.

Sample LZ0602B is a harzburgite with extensive neoblasts. Imaging and EDS maps of fine-grained secondary zones show that secondary phases are silicates and chromium spinels. In all four locations analyzed, silicate phases within these secondary zones are dominated by cations, in order of descending abundance, Mg, Al, Ca, Na, and Fe (Figure 17). The presence of Al and Mg silicates in fine-grained secondary zones shows that these were pyroxene grains that were broken down and recrystallized due to interaction with melt. Oxide phases are chromium spinels. Veins in sample are Al rich-silicate phases. Sodium EDS map and petrography data indicate that Na enrichments can be attributed to infiltrated melt.

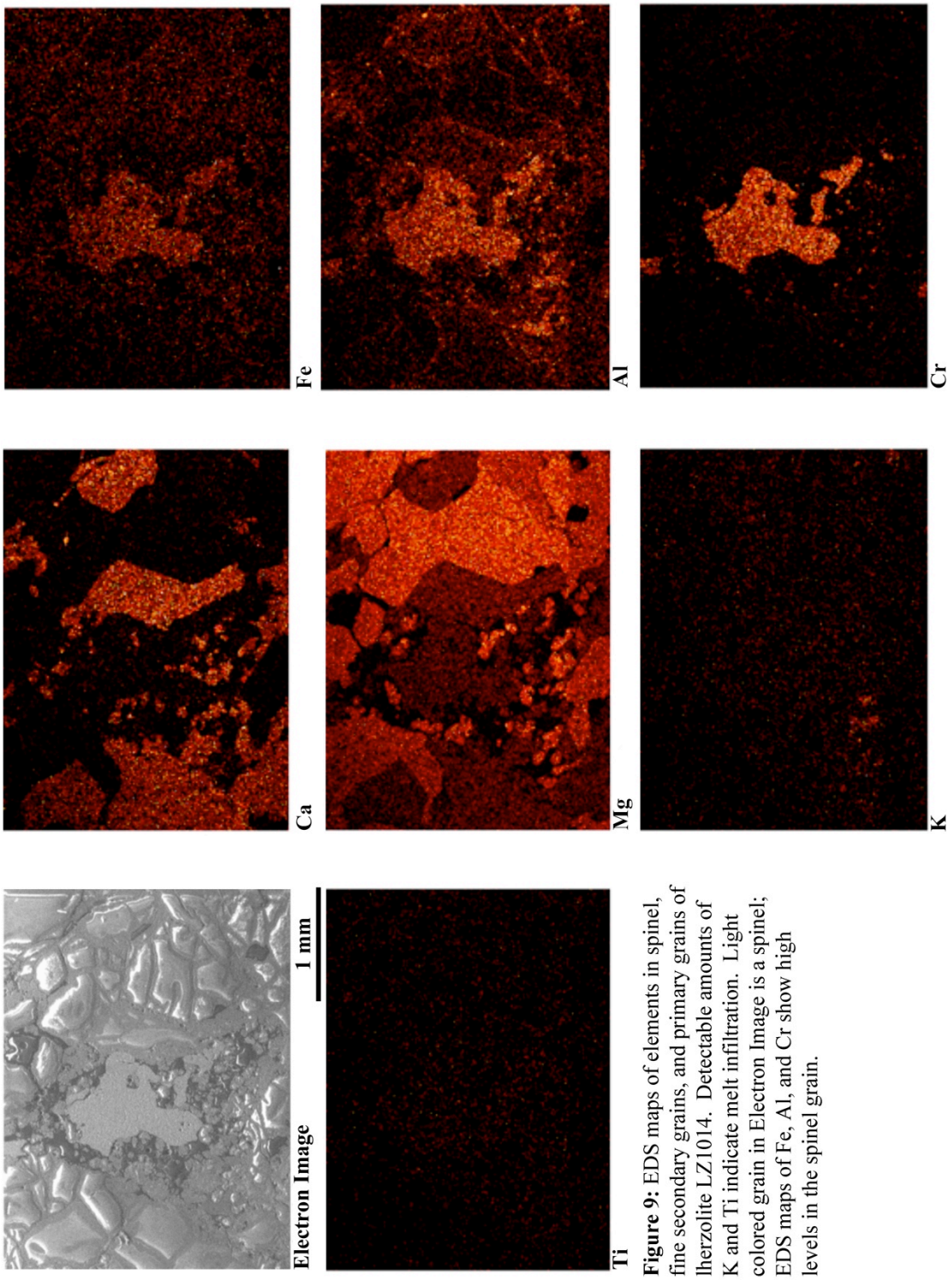

Figure 9: EDS maps of elements in spinel, fine secondary grains, and primary grains of lherzolite LZ1014. Detectable amounts of K and Ti indicate melt infiltration. Light colored grain in Electron Image is a spinel; EDS maps of Fe, Al, and Cr show high levels in the spinel grain.

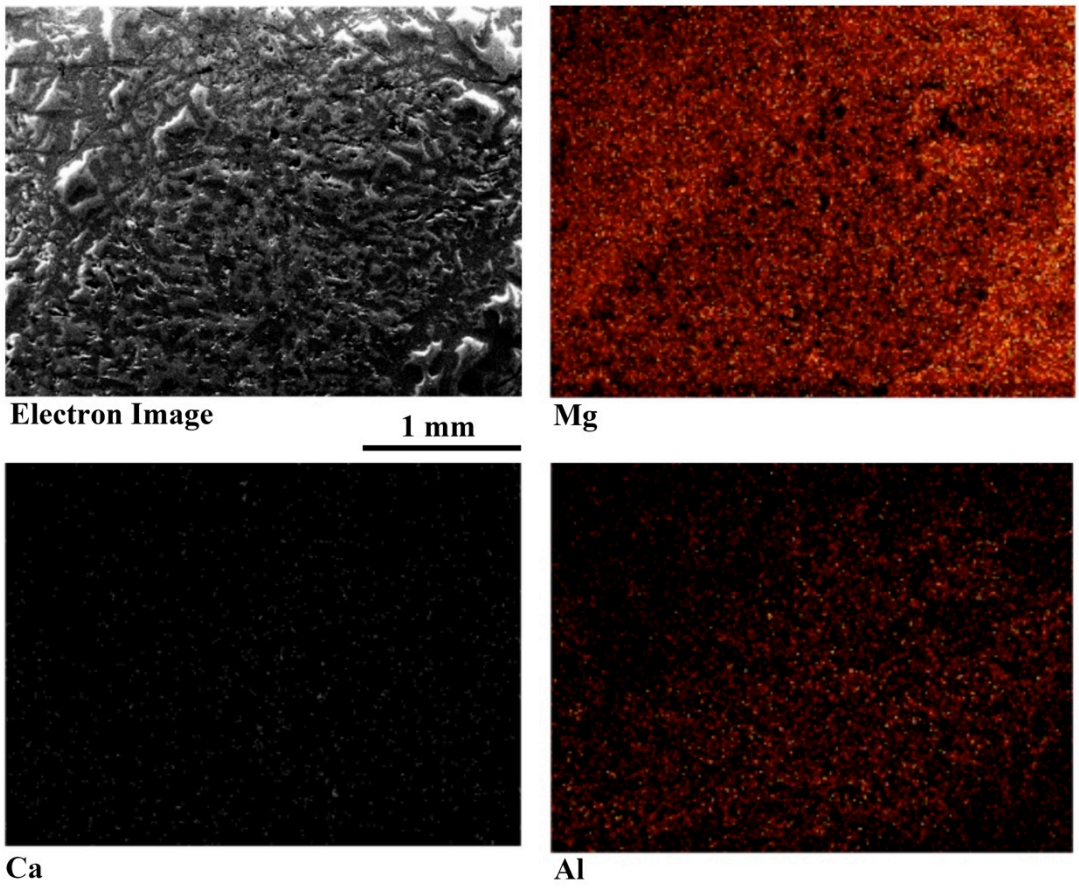

Figure 10: Electron Image and EDS maps of harzburgite sample LZ1016B showing a zone of recrystallized orthopyroxene surrounded by the primary olivine grains (known from petrographic observation).

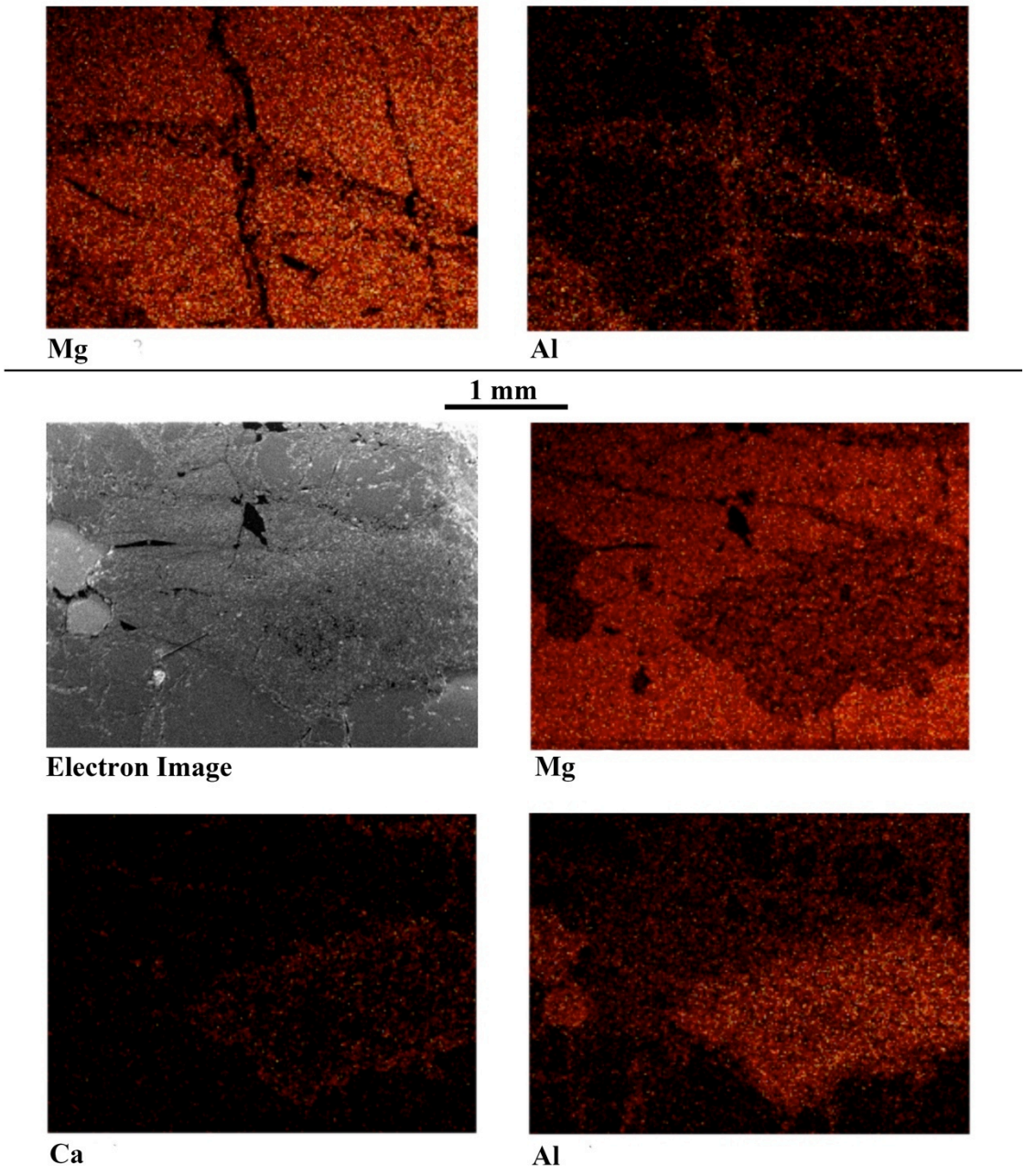

Figure 11: Top–EDS maps showing enrichment of Al in veins of dunite sample LZ1016E; Bottom–high magnesium abundances indicate olivine, secondary zone of Mg, Ca, and Al silicates (Si not shown) indicate that fine secondary grains are Al-rich opx and cpx; Size and shape of secondary zones throughout slide suggest that pyroxenes were primary mineral phases and were subsequently altered to fine-grained pyroxene secondary zones.

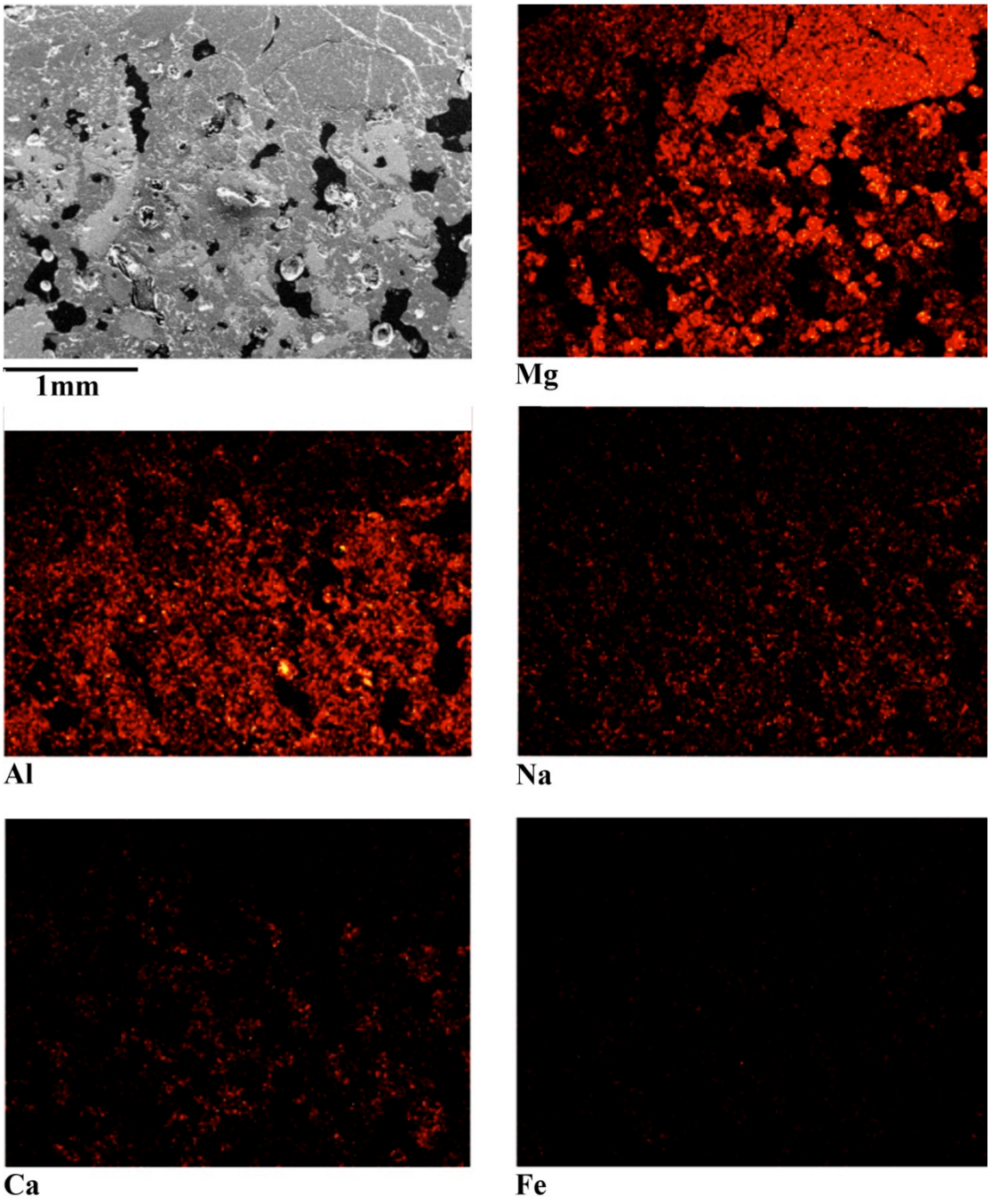

Figure 12: Upper left: electron image of secondary grain-rich zone of sample LZ0602A; other five images are EDS maps of the elements indicated beneath each image. The intensity of red in the images shows high elemental abundances; maps indicate abundances of cations in decreasing order: Mg, Al, Na, Ca, Fe.

Mineral Chemistry

Mineral chemical data obtained using an electron microprobe analyzer were used to calculate equilibration temperatures using multiple geothermometry approaches. Sachtelben and Seck (1981) apply the equation: $T(ºC)=812+163.1x-10.3x^2$, (derived from the experimental data of Lindsley and Dixon (1976), where x=mole % $CaSiO_3$ in orthopyroxene) to determine equilibration temperatures of orthopyroxene-bearing peridotites. Values for equilibration temperatures were obtained using this equation for all orthopyroxene-bearing peridotites. Calculated equilibration temperatures for samples range from 940–1250°C, with an average of 1060°C. On average, intra-sample orthopyroxenes yield variation from the sample average calculated temperature by 90ºC. Of the five dunite samples, none contained primary orthopyroxene grains, and so temperatures could only be calculated using this geothermometer for harzburgite and lherzolite samples. Using the thermobarometry equations of Mercier (1980), equilibration temperatures and pressures were calculated for both cpx and opx grains. For 90% of the samples with equilibration temperatures calculated using both geothermometers, the average temperature per sample calculated using the CaO in opx thermometer of Sachtelben and Seck are higher than those calculated from the Mercier equations (average for cpx and opx when both present for Mercier temperatures). The values from the two geothermometers agree closely, with an average difference of 44ºC, a minimum of 2.4ºC and a maximum of 137ºC. In samples with both opx and cpx EMP data, intra-sample averages of opx and cpx

temperatures average a 39ºC difference, with a minimum of 20ºC and a maximum of 63ºC. In samples with both opx and cpx, average equilibration pressures calculated on cpx are 1.8 to 8.9 kB higher than intra-sample opx averages. Equilibration temperatures and pressures calculated are summarized in Table 3. Sachtelben and Seck geothermometer temperatures of mantle peridotites average at 1060ºC with a standard deviation of 100ºC; Mercier geothermometer temperatures average at 1100ºC with a standard deviation of 90ºC.

Table 3: Thermobarometry data

			Equilibration Temperatures (ºC)				Eguilibration Pressures (kB)		
Sample	Rock Type	Locality[1]	Sachtelben and Seck Average T	Mercier Average T	(M) Average T for opx	(M) Average T for cpx	(M) Average P (all px)	(M) Average P for opx	(M)Average P for cpx
LZ0602A	Harzburgite	3	-	-	-	-	-	-	-
LZ0602B	Harzburgite	3	1003	1040	-	-	10.51	-	-
LZ0603i	Harzburgite	3	1010	1046	1066	1026	19.11	18.23	19.99
LZ0604A	Harzburgite	2	1039	1047	1062	998	20.21	18.73	21.97
LZ0604B	Harzburgite	2	1052	1107	-	-	17.12	-	-
LZ0604C	Harzburgite	2	999	995	-	-	18.27	-	-
LZ0604D	Harzburgite	2	976	1015	1031	998	18.74	17.74	19.74
LZ0605	Harzburgite	4	1239	1248	-	-	21.41	-	-
LZ1001A	Harzburgite	3	961	1014	-	-	16.55	-	-
LZ1001B	Harzburgite	3	1038	1175	-	-	26.37	-	-
LZ1002	Harzburgite	2	1179	1203	-	-	18.84	-	-
LZ1003A	Harzburgite	2	-	-	-	-	-	-	-
LZ1003B	Harzburgite	2	1227	1251	-	-	18.34		-
LZ1003C	Harzburgite	2	1094	1042	-	-	18.67	-	-
LZ1004A	Harzburgite	2	951	1057	-	-	16.16	-	-
LZ1004B	Harzburgite	2	941	1007	-	-	13.53	-	-
LZ1005	Harzburgite	2	964	1069	-		20.30	-	-
LZ1006	Harzburgite	1	1143	1155	-	-	16.02	-	-
LZ1007	Harzburgite	5	965	1018	-	-	20.44	-	-
LZ1008	Lherzolite	5	1015	1082	1073	1112	17.85	17.06	19.42
LZ1009	Harzburgite	5	997	1054	-	-	21.18	-	-
LZ1010	Harzburgite	5	990	1053	-	-	12.41	-	-
LZ1011	Harzburgite	5	946	994	-	-	18.85	-	-

[1]Localities: 1= El Gulfo Maar; 2=Pico Partido; 3= Caldera de Los Cuervos;
4=Montana de Las Nueces 5=El Cuchillo Maar: 6=Guatiza

Table 3: Continued

			Equilibration Temperatures (ºC)				Eguilibration Pressures (kB)		
Sample	Rock Type	Locality[1]	Sachtelben and Seck Average T	Mercier Average T	(M) Average T for opx	(M) Average T for cpx	(M) Average P (all px)	(M) Average P for opx	(M)Average P for cpx
LZ1012A	Lherzolite	5	1035	1072	1090	1055	19.02	15.93	22.11
LZ1012B	Harzburgite	5	1165	1189	-	-	17.19	-	-
LZ1013A	Gabbro	5	-	-	-	-	-	-	-
LZ1014	Lherzolite	5	1022	1087	1078	1098	23.07	19.11	28.01
LZ1015Ai	Troctolite	6	-	-	-	-	-	-	-
LZ1015Aii	Gabbro	6	-	-	-	-	-	-	-
LZ1015Bi	Gabbro	6	-	-	-	-	-	-	-
LZ1016A	Gabbro	6	-	-	-	-	-	-	-
LZ1016B	Harzburgite	6	-	-	-	-	-	-	-
LZ1016C	Plag-Lherzolite	6	-	-	-	-	-	-	-
LZ1016Di	Dunite	6	-	-	-	-	-	-	-
LZ1016E	Dunite	6	-	-	-	-	-	-	-
LZ1016F	Harzburgite	6	1203	1200			18.12		
LZ1016Gi	Gabbro	6	-	-	-	-	-	-	-
LZ1016Gii	Dunite	6	-	-	-	-	-	-	-
LZ1016Hi	Dunite	6	-	-	-	-	-	-	-
LZ1016Hii	Dunite	6	-	-	-	-	-	-	-
LZ1016I	Harzburgite	6	-	1011	-	-	21.67		21.67
LZ1017A	Harzburgite	4	1251	1253	-	-	-	-	-
LZ1017B	Harzburgite	4	1215	1227	-	-	18.32	-	-

[1]Localities: 1= El Gulfo Maar; 2=Pico Partido; 3= Caldera de Los Cuervos;
4=Montana de Las Nueces 5=El Cuchillo Maar: 6=Guatiza

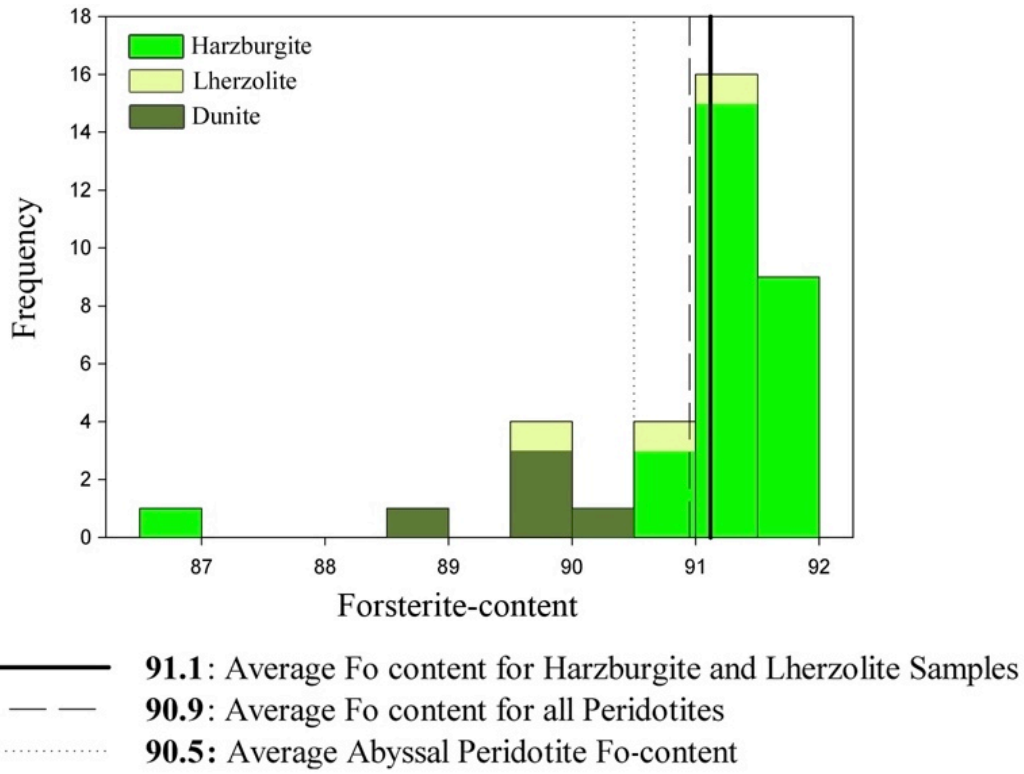

Figure 13: Forsterite content in olivines of peridotites of this study; Average of all peridotites of this study is 90.9; Average of harzburgite+lherzolite samples of this study is 91.1; Average abyssal peridotite Fo-content value of 90.5 from Simon *et al*. (2008) and references therein.

Fo-contents of olivine grains for all peridotites range from $Fo_{86.7\text{-}91.7}$; a histogram of Fo-content is shown in Figure 14 (see Table 4 for summary of mineral chemistries). Also plotted in Figure 14 are lines representing the average values of all peridotite samples, average Fo-content of harzburgite+lherzolite samples, and the average value for abyssal peridotites (from Simon *et al*. 2008), which represents a relatively fertile mantle reservoir. With one single primary orthopyroxene-bearing harzburgite sample, LZ1009, having a Fo value below 90 ($Fo_{86.7}$), the remaining 27 harzburgite samples fall in the narrow range of $Fo_{90.8–91.7}$. Lherzolites fall within the lower range of $Fo_{89.9–91.4}$. Dunite samples have the lowest range of Fo-contents of the peridotites: $Fo_{88.8–90.5}$.

Chromium numbers for all samples with spinels analyzed range from 34 to 73 (range of intra-sample averages) with an average of 53. The average cr# in spinels of harzburgites, at 55, is higher than the overall average. Lherzolite cr#'s average at 50, and dunites have the lowest average cr# of the peridotites at 45. Mg# in spinels of harzburgites range from 48 to 58 . Spinels of lherzolites fall within the range of Mg# of harzburgite spinels, from 57 to 68. Mg# of spinels in dunites range from 42 to 62 (Figure 14). Average TiO_2 wt.% in spinels of each sample were found to range from 0.01 to 0.73 wt.% in harzburgites, 0.16 to 0.35 wt.% in lherzolites, and 0.19 to 0.85% in dunite.

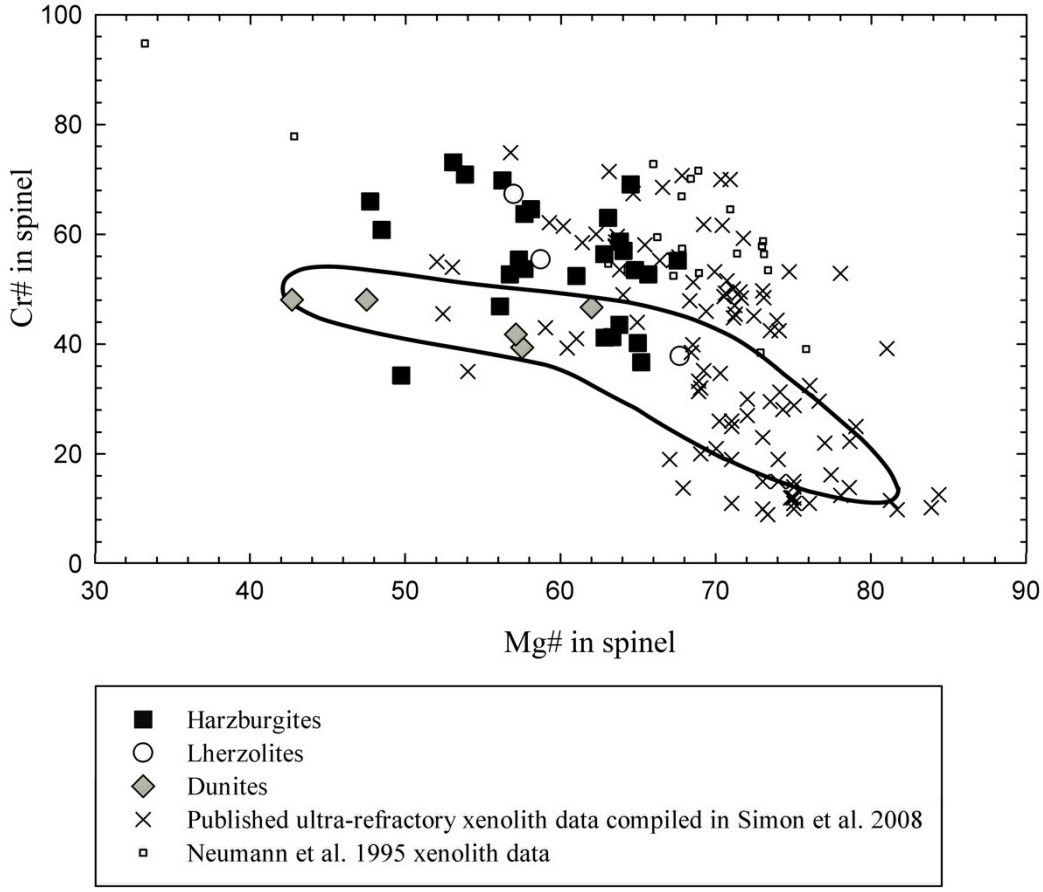

Figure 14: Spinel chemistry Mg# versus Cr# of harzburgite, lherzolite and dunite xenoliths of this study and other published xenolith data; Outlined area is field of melt-depleted abyssal peridotites (from Day *et al.* 2012, Supplementary Figure S7); Majority of Lanzarote xenoliths of this study are more melt depleted than abyssal peridotites (indicated by higher Cr#s). The harzburgite that plots as less depleted/more fertile than abyssal peridotites is sample LZ1009.

For all peridotite samples with primary opx, the range of Al_2O_3 in opx is 0.79-3.09 wt.%. The maximum value is from a lherzolite sample and the minimum value is from a harzburgite. Pyroxenes from porphyroclastic samples have consistently lower Al_2O_3 in opx compared to protogranular samples with pristine pyroxenes.

All but three samples, harzburgite LZ1009, lherzolite LZ1008, and dunite LZ1016Hii, fall within the olivine-spinel mantle array of Arai (1994) plotting forsterite content in olivine against cr# in spinels (Figure 15). Dunites of this study

are consistent with the observations of Arai (1994) in that they plot on the lower forsterite content side of the mantle array. Forsterite content in olivine plotted against TiO_2 wt.% in spinels shows a marked difference in harzburgites and dunites; most harzburgites have a high narrow range of Fo-content and a low (<0.1 wt.%) TiO_2 in spinel, while dunites have a lower range of Fo-content and variable TiO_2 in spinel (Figure16).

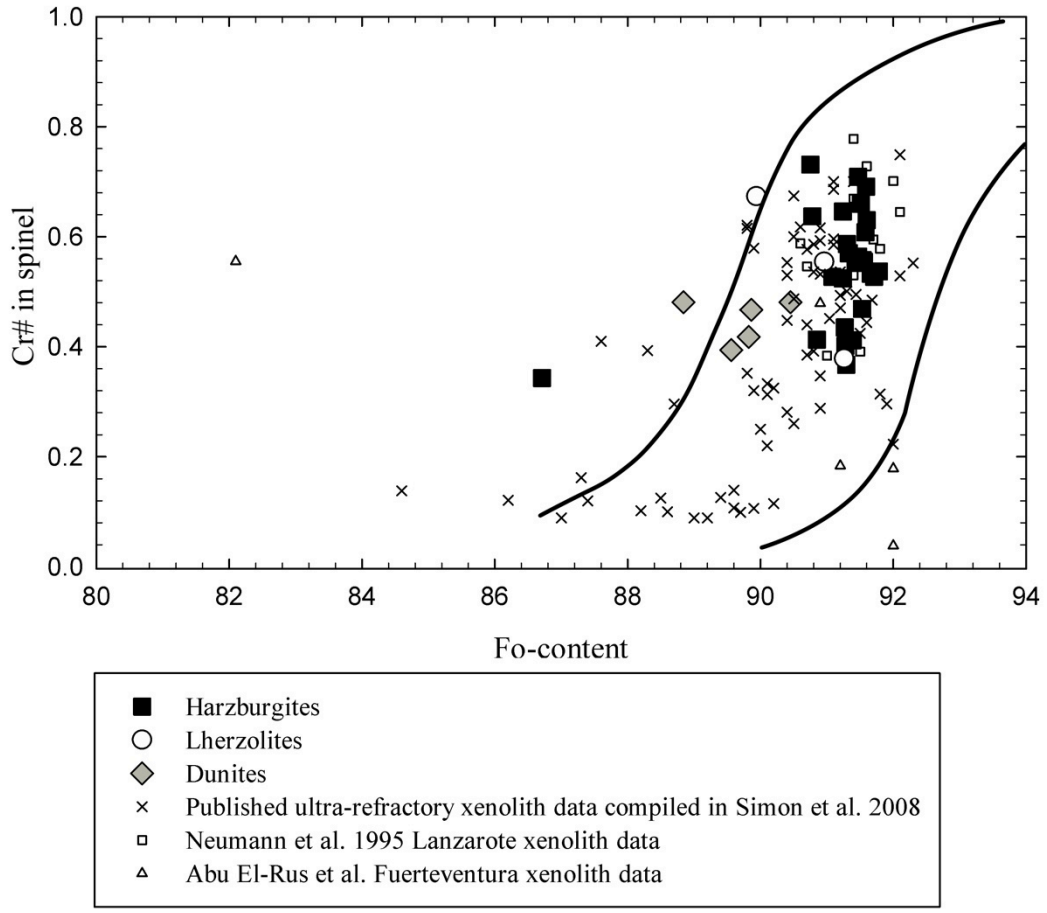

Figure 15: Average forsterite content of olivines plotted against average cr# in spinel for each peridotite sample; lines represent boundaries of the olivine-spinel mantle array of Arai (1994); only three peridotites fall outside the mantle array: dunite LZ1016Hii and harzburgite LZ1009 and lherzolite LZ1008.

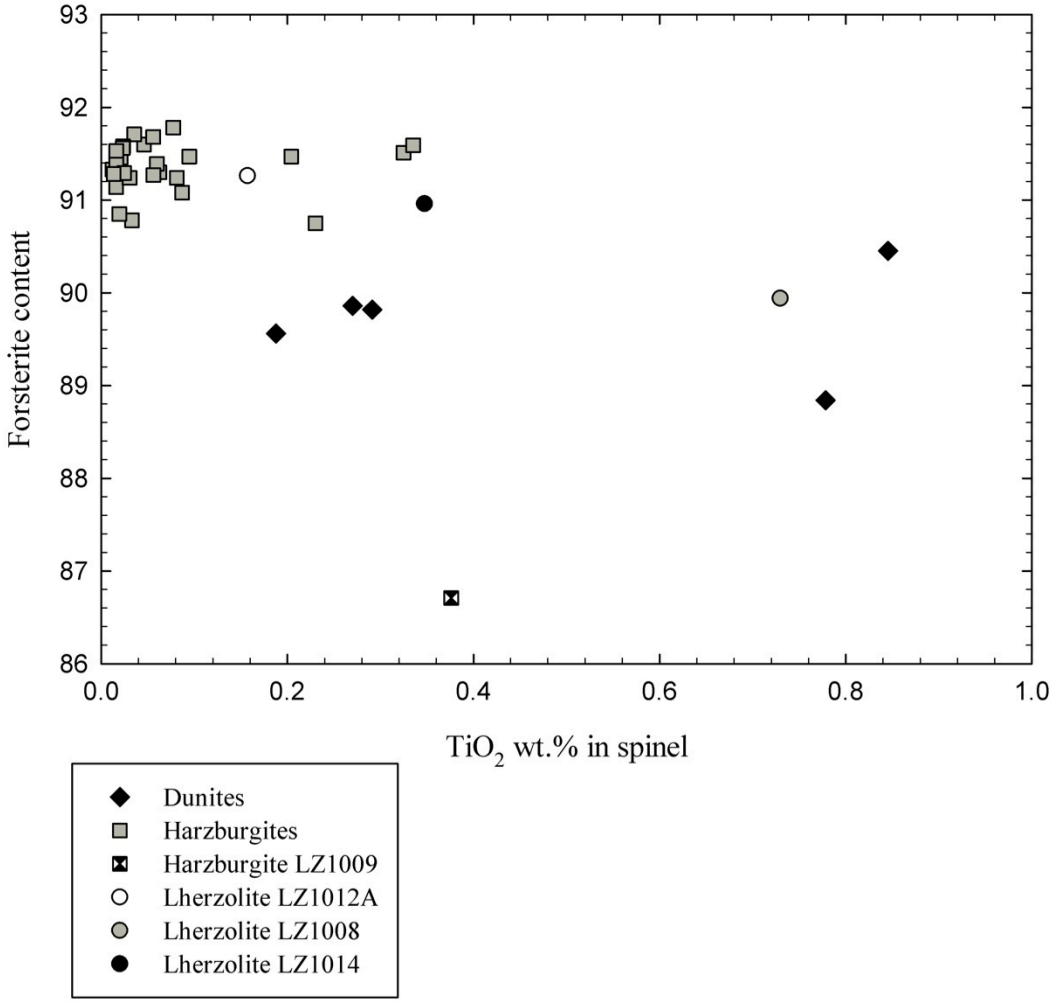

Figure 16: Forsterite contents plotted against TiO_2 wt.% in spinels; Continuing partial melting of a reservoir should drive Fo up and TiO_2 in spinel down (Jaques and Green 1980 and references therein).

Table 4: Fo, cr# in spinel, Al_2O_3 in orthopyroxene, and TiO_2 in spinel

Sample	Rock Type	Locality[1]	Avg. Fo	Avg. Cr# in Spl	Avg. TiO_2 in Spinel[2]	Avg. Al_2O_3 in Opx[2]
LZ0602A	Harzburgite	3	91.14	-	-	-
LZ0602B	Harzburgite	3	91.24	64.6	0.031	1.62
LZ0603i	Harzburgite	3	91.29	36.7	0.025	2.75
LZ0604A	Harzburgite	2	90.85	41.3	0.020	2.35
LZ0604B	Harzburgite	2	91.53	46.9	0.016	2.50
LZ0604C	Harzburgite	2	91.47	70.9	0.095	0.98
LZ0604D	Harzburgite	2	91.28	40.2	0.014	2.35
LZ0605	Harzburgite	4	91.08	52.7	0.087	1.95
LZ1001A	Harzburgite	3	91.47	56.4	0.204	1.65
LZ1001B	Harzburgite	3	91.60	63.0	0.046	1.99
LZ1002	Harzburgite	2	91.30	58.7	0.063	2.08
LZ1003A	Harzburgite	2	91.51	66.0	0.325	-
LZ1003B	Harzburgite	2	91.39	41.2	0.060	3.02
LZ1003C	Harzburgite	2	91.36	-	-	2.59
LZ1004A	Harzburgite	2	91.46	69.8	0.021	1.14
LZ1004B	Harzburgite	2	91.27	43.5	0.056	2.56
LZ1005	Harzburgite	2	91.71	52.7	0.035	2.80
LZ1006	Harzburgite	1	91.58	60.8	0.024	1.99
LZ1007	Harzburgite	5	90.78	63.7	0.033	1.17
LZ1008	Lherzolite	5	89.94	67.3	0.730	1.32
LZ1009	Harzburgite	5	86.71	34.3	0.376	0.87
LZ1010	Harzburgite	5	91.24	52.4	0.081	2.46
LZ1011	Harzburgite	5	90.75	73.1	0.230	0.79
LZ10012A	Lherzolite	5	91.26	37.8	0.157	3.09
LZ1012B	Harzburgite	5	91.68	53.5	0.056	2.00
LZ1013A	Gabbro	5	-	-	-	-
LZ1014	Lherzolite	5	90.96	55.4	0.347	2.05
LZ1015Ai	Troctolite	6	86.45	-	-	-
LZ1015Aii	Gabbro	6	80.37	-	-	-
LZ1015Bi	Gabbro	6	-	-	-	-
LZ1016A	Gabbro	6	85.35	-	-	-
LZ1016B	Harzburgite	6	91.56	55.4	0.023	2.91
LZ1016C	Plag-Lherzolite	6	89.69	-	-	-
LZ1016Di	Dunite	6	89.86	46.7	0.270	-
LZ1016E	Dunite	6	90.45	48.1	0.846	-
LZ1016F	Harzburgite	6	91.33	57.0	0.012	1.93
LZ1016Gi	Gabbro	6	-	-	-	-
LZ1016Gii	Dunite	6	89.56	39.4	0.188	-
LZ1016Hi	Dunite	6	89.82	41.8	0.291	-
LZ1016Hii	Dunite	6	88.84	48.1	0.778	-
LZ1016I	Harzburgite	6	91.78	53.7	0.077	-
LZ1017A	Harzburgite	4	91.59	69.1	0.335	2.11
LZ1017B	Harzburgite	4	91.43	55.2	0.016	2.28

[1]Localities– 1= El Gulfo Maar; 2=Pico Partido; 3= Caldera de Los Cuervos;
4=Montana de Las Nueces 5=El Cuchillo Maar: 6=Guatiza

[2]wt.% oxides in orthopyroxene and spinel

Whole Rock Major Elements

In major element plots, samples are categorized based on petrogrographic observations into the four general categories: harzburgites, lherzolites, dunites, and crustal xenoliths (gabbros, unique troctolite and plagioclase-lherzolite) (Figure 8). In addition to these main rock type categories, harzburgite and lherzolite samples are shown on plots using subcategories including presence of melt infiltration as indicated by the presence of basaltic glass and evidence of melt interaction as indicated by the presence of degraded pyroxenes (porphyroclastic versus protogranular textures) (Figures 9, 10, and 11). These categories are based on the thin section alone; melt infiltration and or degraded pyroxenes may be present in other regions of the sample and not represented in thin section.

For all harzburgite samples whole rock Mg# [$(MgO/(MgO+Fe_2O_3^T)*100$] ranges from 77.4 to 84.7; CaO ranges from 0.4 to 1.0 wt.%; $Fe_2O_3^T$ ranges from 8.30 to 12.5 wt.% and Al_2O_3 ranges from 0.6 to 1.2 wt.%. For lherzolite samples, whole rock Mg# ranges from 81.4 to 83.4; CaO ranges from 1.0 to 2.3 wt.%; $Fe_2O_3^T$ ranges from 8.8 to 10.1 wt.% and Al_2O_3 ranges from 0.7 to 1.3 wt.%. Dunite whole rock Mg# ranges from 79.0 to 81.0; CaO ranges from 0.3 to 1.7 wt.% ; $Fe_2O_3^T$ ranges from 10.5 to 11.8 wt.%; Al_2O_3 ranges from 0.7 to 3.2 wt.%. Crustal xenolith whole rock Mg# ranges from 66.6 to 81.3; CaO ranges from 7.8 to 19.1 wt.%; $Fe_2O_3^T$ ranges from 3.8 to 8.1 wt.% and Al_2O_3 ranges from 4.7 to 22.5 wt.%. Major element XRF data for all samples is given in Table A2.

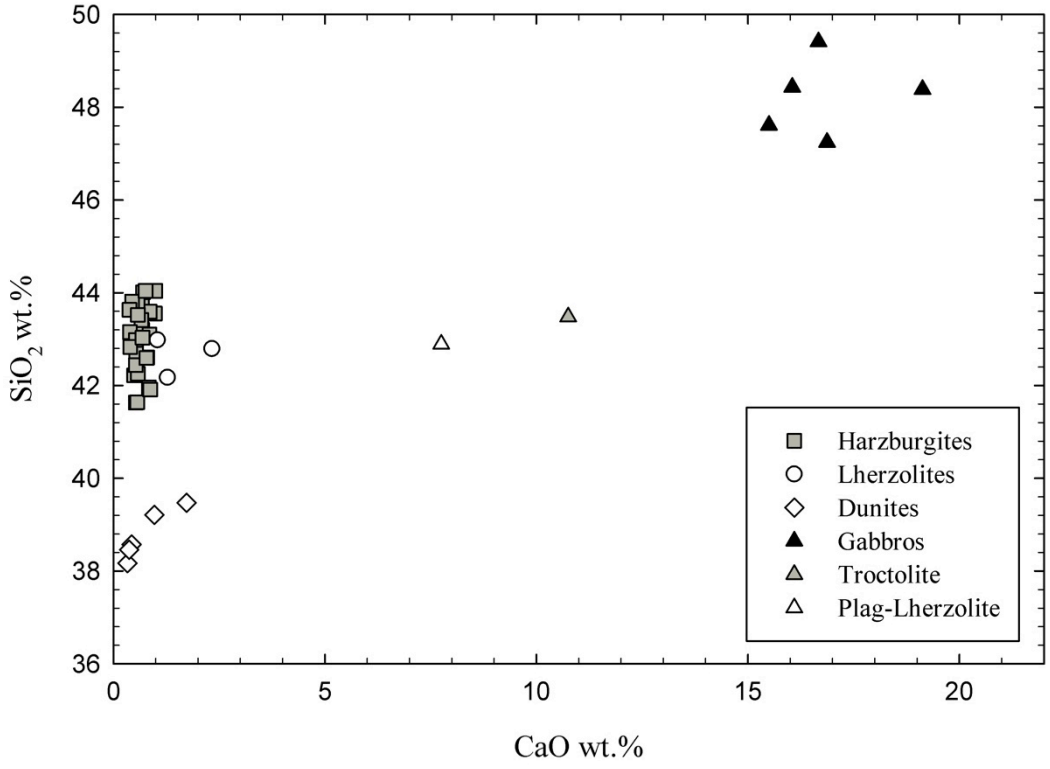

Figure 17: Xenolith whole rock CaO vs. SiO_2 wt.% of all samples.

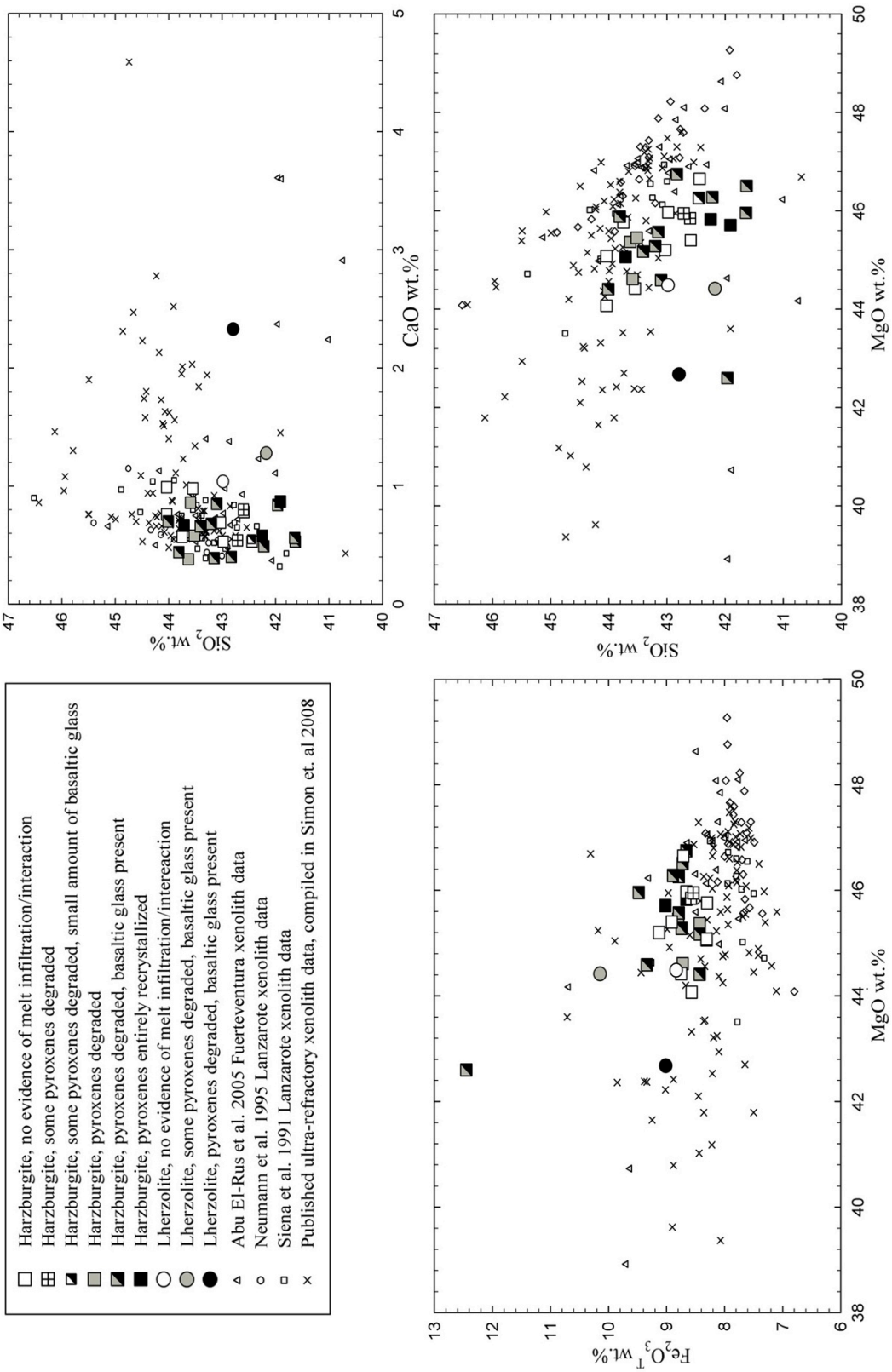

Figure 18: Harzburgite and lherzolite samples of this study as well as selected published data (see key), whole rock major element plots.

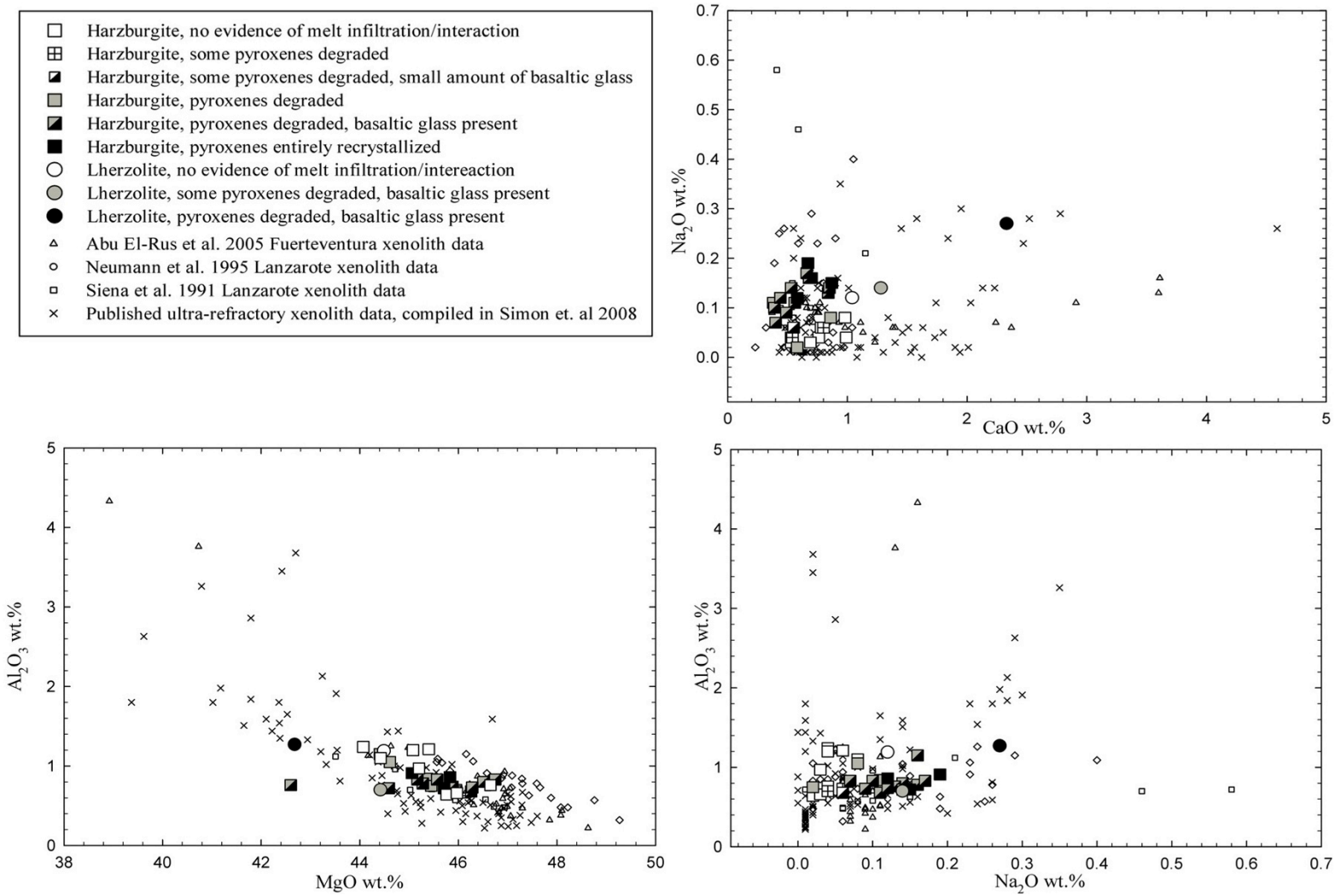

Figure 19: Harzburgite and lherzolite samples of this study as well as selected published data (see key), whole rock major element Al_2O_3 and Na_2O plots.

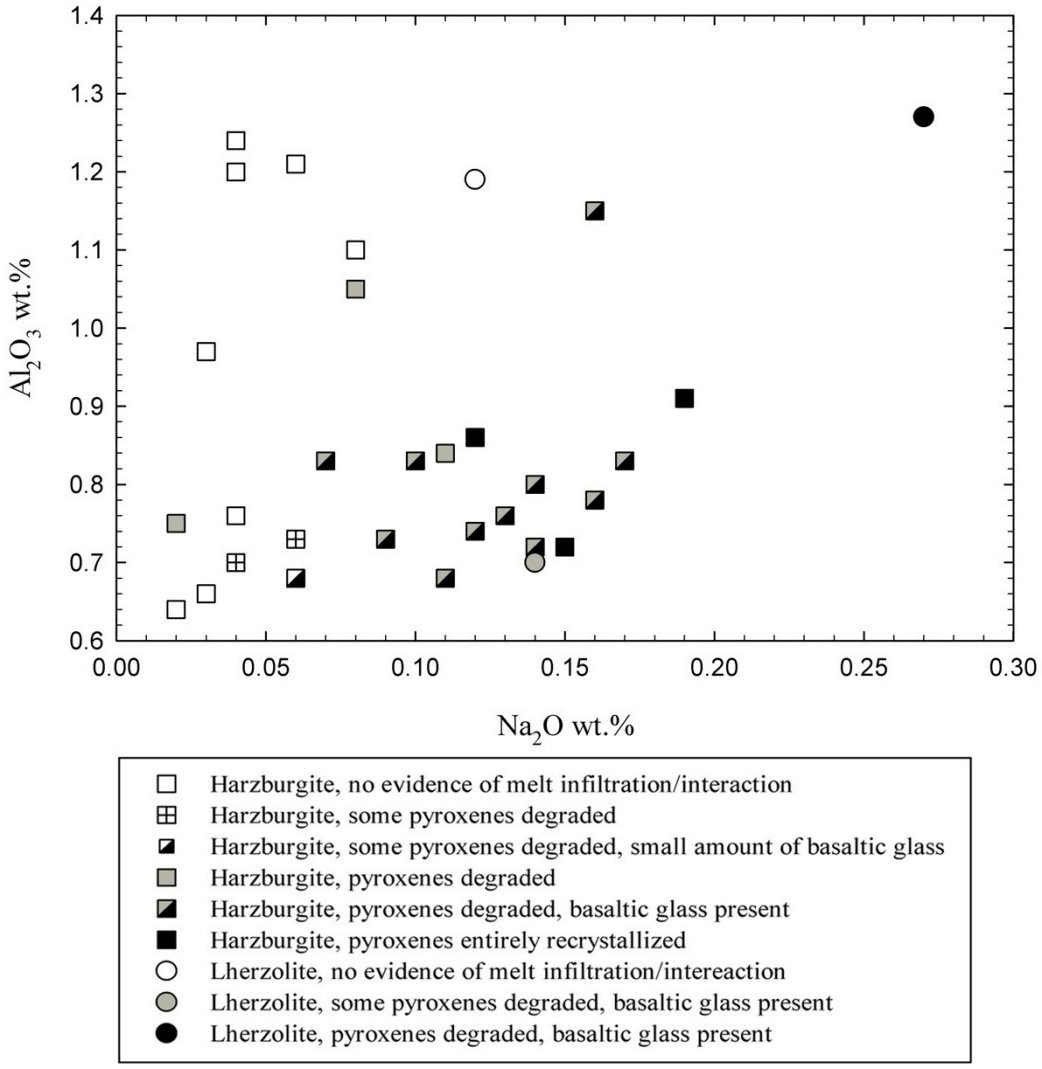

Figure 20: Na_2O wt.% versus Al_2O_3 wt.% in harzburgites and lherzolites of this study only showing an overall trend of increasing Na and decreasing Al for xenoliths with increasing petrographic evidence of melt infiltration+melt interaction.

Whole Rock Trace Elements

Trace elements analyzed by XRF include Rb, Sr, Y, Zr, V, Ni, Cr, Nb, Ga, Cu, Zn, Co, Ba, La, Ce, U, Th, Sc, and Pb (Table A3). Of these, incompatible elements including Rb, Nb, La, Ce, U, Th, and Pb were too often below detection limit to see any meaningful variations and are not considered further. The remainder of the trace elements show meaningful variation, some being enriched in mantle xenoliths, some being variable across the lithologies, and others being enriched in crustal xenoliths (Figures 11 and 12). Yttrium and Gallium were below detection limit for some peridotite samples, but are still presented here showing enrichment to the point of detection broadly correlating with petrographic observation (Figure 13).

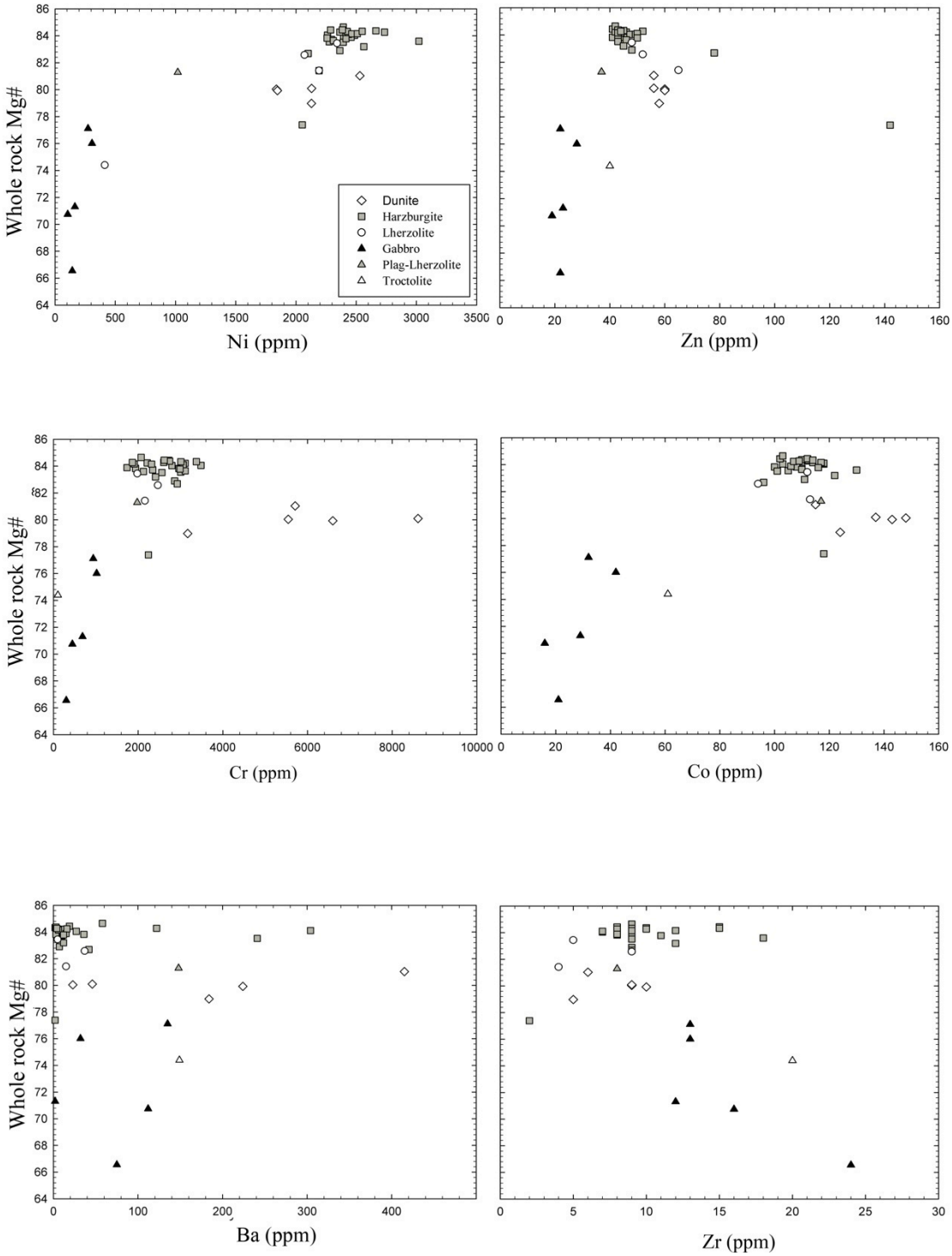

Figure 21: Plots of trace elements versus whole rock Mg#; Left axis label and scale apply across sets of plots; Ni, Zn, Cr, and Co are more enriched in mantle xenoliths; Ba and Zr are variable for all rock types (data is unavailable for some low abundance trace elements for some LZ06* samples, see Table A3).

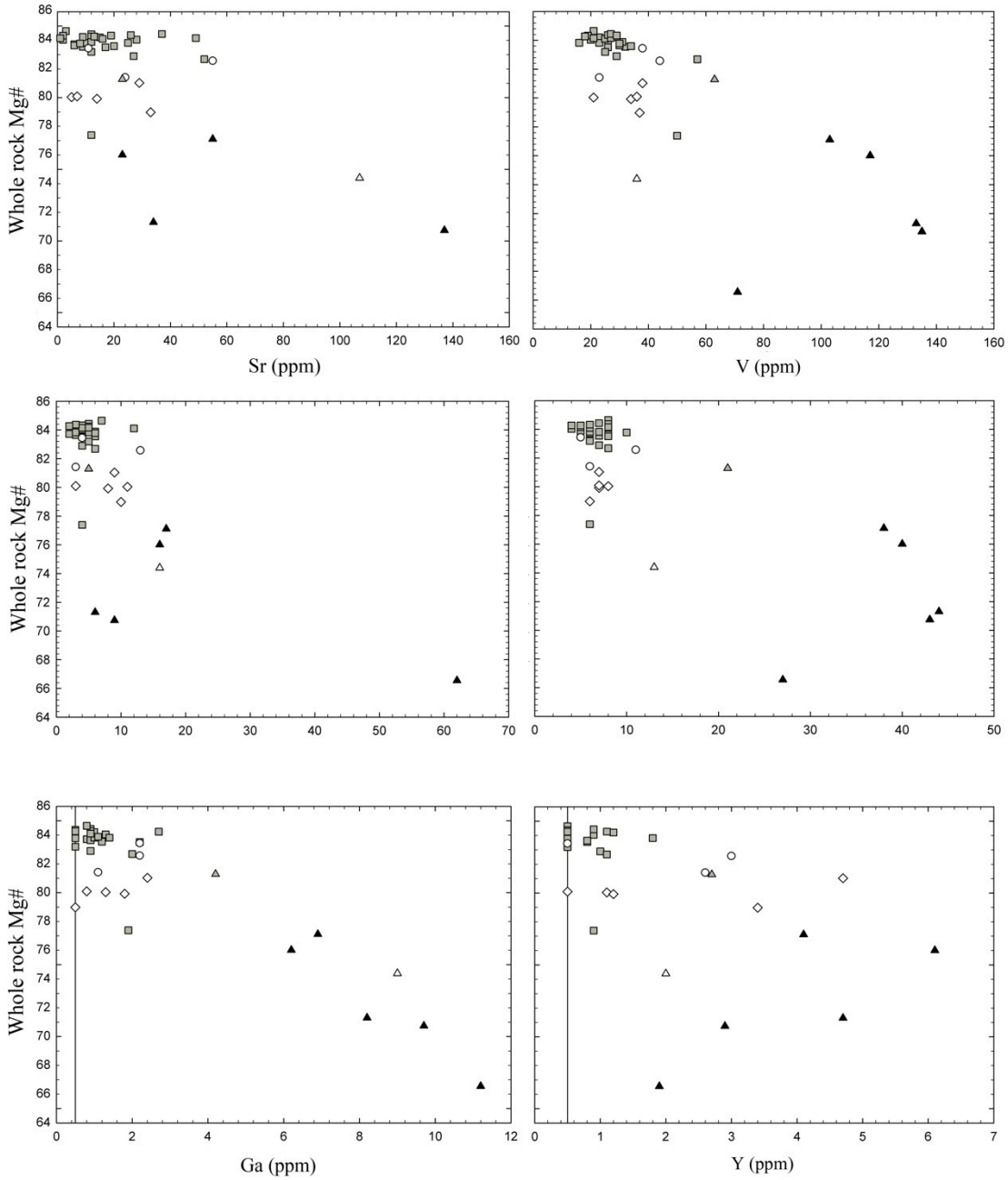

Figure 22: Plots of trace elements versus whole rock Mg#; Left axis label and scale apply across sets of plots; One gabbro sample has a Sr value of >800 ppm, and so is excluded from the plot in order to show variation among all other samples; Ga and Y are below detection limit for some samples, measurements below detection limit are all plotted at the line representing detection limit, 0.5 ppm for both elements (data is unavailable for some low abundance trace elements for some LZ06* samples, see Table A3).

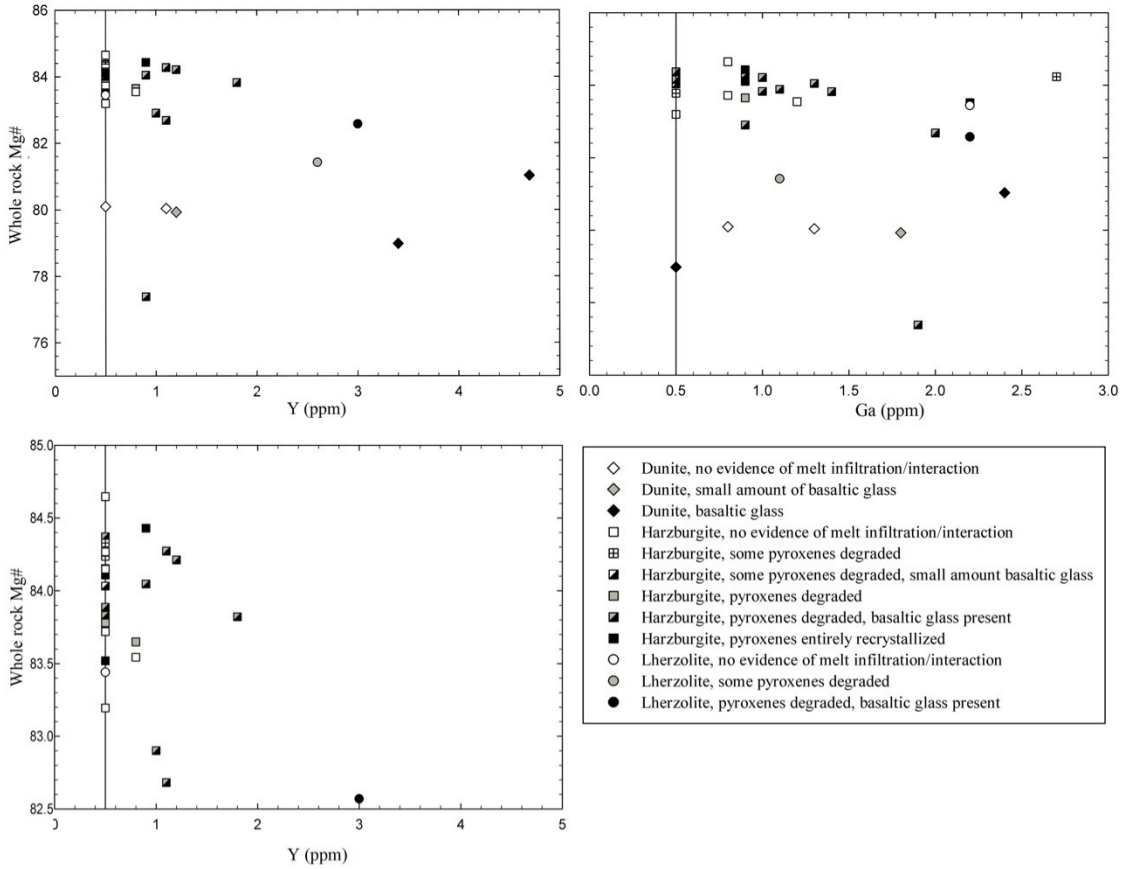

Figure 23: Plots of Y and Ga versus whole rock Mg# for all harzburgites, lherzolites, and dunites showing petrographic distinctions; Bottom left is a zoomed in plot of Y versus whole rock Mg# to show which petrographic categories of rocks have the lowest Y abundances (data is unavailable for some low abundance trace elements for some LZ06* samples, see Table A3).

DISCUSSION

Cross-Island Variability and Constraints

Field and laboratory observations show that not all type-sources are sampled at all vents. At Caldera de Los Cuervos, for example, no crustal xenoliths were collected or observed. El Golfo Maar had rare crustal xenoliths. Pico Partido, and El Cuchillo Maar were observed to have abundant mantle and crustal xenoliths. Guatiza is also the only location with spinel-dunites for this xenolith suite. This may be due to sampling shortcomings, but since dunites were neither collected from nor observed at other localities, these dunites most likely represent a source not sampled by the other cones and maars of this study. Higher calcium and larger vol.% clinopyroxene are found in some peridotites from El Cuchillo Maar. Chemical and textural evidence show that this may be due in part to re-fertilization processes. A very important spatial relationship of this xenoliths suite is that harzburgites of this xenoliths suite show no significant variation in terms of textures, whole rock chemistries, or mineral chemistries at different localities across the island; the refractory harzburgite-composition reservoir beneath Lanzarote represented by xenoliths of this study appears to be notably homogenous.

Xenolith emplacement mechanisms applied to Lanzarote xenoliths

The process by which xenoliths are emplaced in eruptive material is described in detail by Klugel (1998). Klugel's 1998 study focuses on a suite of xenoliths from the 1949 eruption on La Palma, Canary Islands. The process of emplacement begins

when peridotitic wall-rock is broken off due to hydraulic fracturing associated with melt and becomes entrained in an ascending magma. Based on settling rate, ultramafic xenoliths 15 cm in diameter require an ascent rate of ≥ 0.2 ms^{-1} to transport them from their source to crustal depths in alkali basaltic melts (Klugel, 1998; Spera, 1984). As the xenolith ascends suspended in the magma, fractures form from tensions within the xenolith associated with decompression. These fractures can become infiltrated by melt and may become the new xenolith surface, giving rise to varied exposure times at xenolith-host interfaces determined by Klugel (1998) via diffusion calculations. Early formed fractures are distinguished from late formed fractures by the presence of melt. Shapes of xenoliths are controlled by dissolution and/or ablation yielding rounded surfaces, and fragmentation due to decompression yielding angular surfaces (Klugel, 1998; Sachs & Stange, 1993). Klugel (1998) proposes a two-stage ascension for xenoliths of La Palma, Canary Islands: stage one is ascension from their source at ~35 km depth to crustal depths of 7-11 km taking just 37 hours transport time or less; diffusion across xenolith-host interface shows that xenoliths were stored in this crustal reservoir for up to several years before a 4 day transit to the surface during which stagnation must have occurred to prolong the otherwise 9 hour maximum transit time needed to go from crustal depths to the surface while keeping the xenoliths in suspension. Xenoliths of this study are typically much less than 15 cm across, with the largest being approximately 15 cm, and have approximate densities (calculated density for representative harzburgite: ~3.2 g/cm^3) that yield a xenolith-magma density difference of less than 0.5 g/cm^3 between xenolith and alkaline basalt

melt; it can therefore be assumed that magma ascent rates calculated for ultramafic xenoliths of the Klugel (1998) study would also be sufficient to transport all crustal and mantle Lanzarote xenoliths studies here.

Crustal samples

The five gabbros, the troctolite, and the plagioclase-lherzolite represent crustal material being sampled by Lanzarote volcanism. The troctolite sample, by definition, represents a cumulate rock. The textures of plagioclase-bearing lherzolite lZ1016C suggest that it too is a crustal cumulate. The gabbros of this study have similar textures, mineralogies, and whole rock major chemistries to Lanzarote MORB-type gabbro cumulate xenoliths of Schmincke *et al*. (1998) and Neumann *et al.* (2000) sourced from the Jurassic-age oceanic crust underlying the island. No fractures were observed in crustal xenoliths, consistent with the lower amounts of decompression that a shallower sourced rock would undergo during transit to the surface. As with the mantle xenoliths, crustal xenoliths show petrographic evidence of varying extents of melt infiltration and interaction; the troctolite sample exhibited the most extensive amount of secondary grain formation and basaltic melt infiltration.

Mantle peridotites–Re-fertilization Effects

Major element whole rock chemistries are generally unaffected by melt interaction and the small volume amounts of melt infiltration observed in the harzburgite group. One exception to this is sodium. Harzburgites with no evidence of

melt infiltration or interaction have Na_2O wt.% from 0.02 to 0.08 with an average of 0.04 wt.%. Harzburgites with both degraded pyroxenes indicating melt interaction and infiltration of basaltic glass observed in thin section have Na_2O from 0.07 to 0.17 wt.% with an average of 0.13 wt.%. Porphyoroclastic, high Na harzburgites also tend to have lower wt.% Al_2O_3, consistent with the lowered mineral chemistry Al range in orthopyroxenes of porphyroclastic harzburgites as compared to the range of Al mineral chemistries in orthopyroxenes of protogranular harzburgites. Siena *et al*. (1991) report ranges for Al_2O_3 wt.% in primary orthopyroxenes and 'spongy' pyroxenes. These 'spongy' pyroxenes correspond to pyroxenes in this study reported as 'degraded.' Primary pyroxenes from this study fall within the range reported for primary pyroxenes of Siena *et al*. (1991); degraded pyroxenes from this study constitute a wider range than reported for the Siena *et al.* study's 'spongy' pyroxenes, but are consistent with their results in that these degraded pyroxenes have a much lower range than that of primary pyroxenes in protogranular samples.

Continued partial melting of a reservoir is expected to drive Fo up and TiO_2 in spinel down (Jaques & Green, 1980). All protogranular harzburgites retain their refractory mineral chemistries with respect to Fo-content and TiO_2 in spinels with Fo-contents above $Fo_{91.3}$ and TiO_2 below 0.1 wt.% with the exception of sample LZ1017A; many porphyroclastic samples also retain their refractory olivine and spinel mineral chemistries, all having Fo-content over $Fo_{90.7}$ and many with TiO_2 in spinel below 0.1 wt.%. Harzburgites with significantly elevated TiO_2 in spinel include LZ1001A, LZ1003A, LZ1011, LZ1017A, and LZ1009. With the exception of sample

LZ1017A, these samples were also observed to have highly degraded pyroxene as well as the presence of basaltic glass. Sample LZ1017A, while it did not have significantly degraded pyroxene and had no basaltic glass present in thin section to indicate interaction with melt, it did contain small amounts of secondary grains. Harzburgite LZ1009 again shows marked chemical variation from the rest of the harzburgites. Although sample LZ1009 shows evidence of both melt interaction and melt infiltration, the large difference in mineral chemistries to those of other porphyroclastic harzburgites suggests that this is not just a re-fertilization effect but reflects a significantly different source chemistry. High titanium levels in spinel and Fo-content of dunites LZ1016E and LZ1016Hii indicate re-fertilization compared to other dunites, consistent with the fact that these are the only two spinels that contain significant amounts of infiltrated basaltic glass.

The three lherzolites each appear to have different source characteristics. Lherzolite LZ1014 has mineral chemistries of $Fo_{91.4}$, falling within the upper half of the narrow range of the harzburgite samples ($Fo_{90.75–91.71}$ excluding LZ1009) but with TiO_2 up to 0.6 wt.% in spinel, which is considerably higher than that most harzburgite samples (which have an average of 0.08 wt.% TiO_2 in spinel). This could be due to re-fertilization processes, which would be consistent with this sample's unique texture (large cpx, secondary, and basaltic glass-rich vein). Olivines in these samples are on the order of 10 times as large as typical spinels, so it is intuitive that the cores of olivines would not be as effected by re-fertilization processes as those of spinels. Lherzolite LZ1008, with strong evidence of melt infiltration and interaction, has low

$Fo_{89.5}$ and high (0.6-1.0) TiO_2 wt.% in spinels that suggest it was not only re-fertilized, but also is sourced from a reservoir that had undergone smaller degrees of partial melting than the reservoir represented by the harzburgite samples; this interpretation is consistent with the fact that this sample exhibits only some degraded pyroxenes, so should not have TiO_2 levels in spinels drastically different from the harzburgites and lherzolites if it was merely material from the same reservoir that has been re-fertilized. Lherzolite samples LZ1014 and LZ1008 have significantly more vol.% clinopyroxene than any ultramafic xenolith reported in either the Neumann *et al*. (1995) or the Siena *et al*. (1991) study. Protogranular lherzolite LZ1012A is expected to have source-representative mineral chemistries, as its textures suggest no re-fertilization effects.

Samples LZ1003A, LZ1016B, and LZ1016I have anomalous textures that are not reported in the Neumann *et al*. (1995) or Siena *et al*. (1991) studies. The recrystallization of orthopyroxenes has little effect on most major elements, with the exception of sodium and aluminum, which are respectively enriched and depleted compared to protogranular harzburgites.

Most trace elements measured, Sc, Co, Zn, Ga, Cr , Ni, V, and Y show a distinct enrichment in either crustal or mantle xenoliths; Ba and Zr are more variable among all rock types; Cu and Sr are most enriched in crustal xenoliths but show significant overlap with mantle xenoliths. Of the elements that exhibit clear distinction between crustal and mantle samples, Ni, Cr, Co, and Zn are high in mantle material. This can be attributed to the high modal proportions of olivine (Ni, Cr, Co) and significant amounts of spinel (Zn), which these elements are known to be

incorporated into (*e. g*. Kenedy *et al.,* 1993; Horn *et al*., 1994). Sc, Ga, V, and Y are enriched in crustal xenoliths. Sc and V are also present in all mantle xenoliths in detectable amounts. Y and Ga, on the other hand, are very low in xenoliths with no evidence of melt infiltration/interaction. Y is below detection limit for eight of the nine protogranular harzburgites and the one protogranular lherzolite. Protogranular harzburgite LZ1003C, the only protogranular harzburgite with detectable levels of Y, also has the highest Na content of all protogranular harzburgites, implicating that there is likely melt infiltration and or interaction in part of the xenolith analyzed for whole rock major and trace elements that it not represented in thin section. Therefore, of the trace elements analyzed, Y represents the most sensitive tracer to melt interaction and infiltration in these mantle xenoliths.

Mantle Peridotites–Melt depletion

The majority of the mantle xenoliths analyzed in this study are harzburgites with highly refractory chemistries with respect to whole rock major element and primary mineral chemistries. Some have been altered by metasomatism and interaction with melt, but analyses of the cores of olivines, orthopyroxenes, and spinels show that their protoliths had refractory chemistries similar to the less altered refractory xenoliths. As discussed above, mineral chemistries of spinels in some samples with petrological evidence of melt interaction exhibit re-fertilization. Of the harzburgite mantle xenoliths of this suite, protogranular samples LZ1003B, LZ1016F, LZ1017B, LZ0603i, LZ0604A, LZ0604B, and LZ0604D were determined to have the

most source-representative textures, mineralogies and refractory chemistries and provide the best insight to understanding the texture, mineralogy, and chemistry of the refractory mantle reservoir beneath Lanzarote. Protogranular harzburgites LZ1017A and LZ1003C are excluded from this based on their re-fertilized mineral and whole rock chemistries, respectively. Only one harzburgite sample, LZ1009, was found to be significantly more fertile with an average Fo-content of $Fo_{86.7}$. Whole rock and mineral chemistries of sample LZ1009 are markedly different from other harzburgites. Sample LZ1009's Fo-contents fall well outside the ranges of all other xenoliths reported from this study, the Neumann *et al*. (1995), and the and Siena *et al*. (1991) study combined. This porphyroclastic harzburgite sample does not show any significant textural differences from other porphyroclastic harzburgites, and it can therefore be assumed that the low Fo-content in this sample is characteristic of its protolith, which represents a less depleted reservoir that has been sampled by Lanzarote volcanism.

Lherzolite LZ1012A, with protogranular texture, has Fo-content similar to the harzburgites, but significantly higher TiO_2 in spinel (average 0.16 wt.%). This sample is therefore interpreted to represent the more fertile-type reservoir that protogranular harzburgites evolved from through continued partial melting. The mineral chemistries of the protogranular dunite group have consistently lower Fo-content and higher TiO_2 wt.% in spinel than the refractory harzburgites. Therefore the mineral chemistries show that the dunites are not related to the harzburgites through partial melting and are less refractory than the harzburgite group.

Most harzburgites of this xenolith suite fall under the ultra-refractory category of Simon *et al*. (2008). Several harzburgites have slightly more than 3 vol.% clinopyroxene but are otherwise consistent with the ultra-refractory group. Sample LZ1009 is the only harzburgite that consistently outside of the ultra-refractory group for multiple criteria. Lherzolite LZ1012 falls within the ultra-refractory group for all chemistries analyzed, but has higher vol.% cpx. Lherzolite LZ1008 is best classified as the fertile group of Simon *et al*. (2008). Lherzolite LZ1014 has olivine and spinel mineral chemistries consistent with the ultra-refractory group, but the abundance of clinopyroxene and related high CaO content classify this sample as the fertile group of Simon *et al*. (2008). Equilibrations temperatures calculated for xenoliths of this study fall within ranges reported for other ocean island peridotite equilibration temperatures from Simon *et al*. (2008), Neumann (1991), and Neumann *et al*. (1995).

The mineral chemistries of this suite of xenoliths mostly overlap those reported in these two previous studies of Lanzarote ultramafic xenoliths. Notable consistencies include the mineral chemistry-based conclusion that the dunites of both this suite and the Neumann *et al*. (1995) suite are not related to the harzburgites by increased extents of partial melting. Also notable is the depletion of Al_2O_3 wt.% in altered orthopyroxenes of this study and of Siena *et al*. (1991).

Implications for understanding mantle composition and ultra-refractory mantle

Harzburgites of this study were determined to represent two different mantle sources. Harzburgite LZ1009 represents a less refractory reservoir, while all other

harzburgite samples, with high narrow range of Fo-content, and low narrow range of TiO_2 in unaltered spinels, represent a highly refractory source reservoir being sampled across the island of Lanzarote. Lherzolite LZ1014 is likely a strongly re-fertilized xenolith with a protolith similar to the protogranular harzburgites and likely represents the same source. Protogranular lherzolite sample LZ1012A represents a slightly less refractory source than the protogranular harzburgites; Lherzolite LZ1008 is a re-fertilized lherzolite but with a protolith significantly more fertile than the protogranular harzburgites.

Re-fertilization processes, for the most part, have minimal effects on major element compositions of ultra-refractory xenoliths. The only exception to this is lower abundance major elements Na and Al. Geodynamical properties of ultra-refractory reservoirs would not be significantly affected by the slight chemistry changes caused by re-fertilization processes that have altered xenoliths of this study with perhaps the exception of sample LZ1014, which likely has a significantly different mineralogy than its ultra-refractory protolith. Re-fertilization processes more strongly affect trace element chemistries as well as mineral chemistries, especially of spinels.

Twenty-eight of the thirty-five mantle xenoliths of this study spanning the island of Lanzarote were found to represent a depleted, ultra-refractory mantle reservoir. Yet Canary Island lavas have been found to be sourced from an enriched mantle reservoir (*e.g.*, Day *et al.,* 2010). Ultra-refractory xenoliths of Lanzarote therefore must represent a reservoir shallower than the enriched magma source that is being sampled as magmas ascend to the surface. This can be supported by the

physical properties of ultra-refractory mantle material, having low densities driving residues to the uppermost parts of the mantle, and high solidus temperatures (Simon *et al.,* 2008) making them impervious to further melting, at least under the conditions that are causing the melting of a deeper reservoir to generate Canarian magmas (Schmincke, 1982; Hoernle & Schmincke, 1993).

Future work and considerations

Trace element measurements were done by XRF, and do not have detection limits below 0.5 ppm for any of the elements analyzed. It is likely, based on observations made here, that some trace elements like Y, as well as others that were too low for detection via XRF, provide a good tracer for alteration of low abundance chemistries of mantle material. An obvious next step for continued study of this xenolith suite would be to do high precision Inductively Coupled Plasma–Mass Spectrometry (ICP-MS) trace element analyses. To better understand the mineralogical controls on trace element enrichment in these xenoliths, mineral-separate trace element analyses on representative samples by ICP-MS is also planned.

The refractory xenoliths of this study represent a mantle reservoir that has undergone large degrees of partial melting. Partial melting is known to cause highly siderophile element (HSE: Os, Ir, Ru, Pt, Pd, Re) fractionation (Barnes *et al*., 1985; Rehkamper *et al*., 1999). HSE analysis, for this reason, is also a vital future step in understanding the origin of this xenoliths suite. This will give powerful insight to the effects of high degree partial melting on residues and HSE distribution in mantle

reservoirs. It is also important to establish the age of melt-depletion events for the mantle reservoirs sampled by Lanzarote volcanism in order to better understand terrestrial mantle evolution. Melt-depletion event ages are best established by using the ^{187}Re–^{187}Os system (Rudnick & Walker, 2009; Coltorti *et al.*, 2010; Creaser *et al.,* 1991); this system's usefulness is due to the fact that Re is incompatible and Os is compatible during melt-extraction (Morgan; *et al.,* 1999). Simon *et al.* (2008) conclude that Os model ages of many ultra-refractory peridotites reflect ancient melting events, and that the formation of ultra-refractory mantle reservoirs is unrelated to island-formation processes. Some Canarian lavas have been found to have unradiogenic Os signatures that are attributed to contamination by the presence small amounts of disaggregated mantle xenoliths (Widom *et al*., 1999). So, although ultra-refractory mantle reservoirs are likely not the source of the lavas in these settings, the chemistries of the lavas themselves can reflect the presence of ancient melt-depleted residues. While Os isotope measurements can serve as a blunt chronometer, they can be coupled with trace elements to understand the evolution of depletion and melt-rock reaction of mantle reservoirs being studied here.

The homogeneity of the highly refractory source reservoir represented by twenty-seven of twenty-eight harzburgite xenoliths of this study is a striking characteristic of the mantle beneath Lanzarote. In order to investigate further the spatial extent of this reservoir, as well as any variability in metasomatic and re-fertilization processes, it is imperative to expand on the xenolith suite reported here. For this reason, the 2012 field campaign (conducted by Day and Traver) aimed to

collect more samples from xenolith localities previously targeted for sampling, as well as search for other xenolith-bearing eruptive material. The spatial range of the xenolith suite was greatly expanded by sampling xenoliths from cones of northern Fuerteventura, which lie approximately 30 km south-west of the nearest Lanzarote sample location. Abu El-Rus *et al.,* (2006) report fibrous orthopyroxene textures interpreted as serpentinization and subsequent dehydration of the upper mantle during the formation of Fuerteventura. To understand of the extent of the homogenous refractory mantle reservoir being sampled across Lanzarote, it will be crucial to investigate Fuerteventura samples and quantify the depleted nature of their source reservoir(s). A comparison of samples from both islands will also likely give insight as the cause of highly variable alteration styles. Analyses executed for this study, as well as the planned future analyses will also be carried out on new Lanzarote and Fuerteventura samples of the 2012 collection campaign.

CONCLUSIONS

Harzburgites of this study, with the exception of more fertile sample LZ1009, reflect a highly refractory deformed mantle source-reservoir with striking homogeneity across the sampling sites. These xenolith samples exhibit a high narrow range of $Fo_{90.8\text{-}91.7}$, cr# in spinel from 37-73, whole rock Mg# ranging from 82.7-84.7, whole rock CaO ≤1.0wt%, and whole rock Al_2O_3 ≤1.3 wt.%. Of these, protogranular harzburgite xenoliths with low Na_2O wt.%, and the lowest Yttrium abundances likely have chemistries that are the most representative of the refractory source reservoir. Textural and chemical trends suggest that some of the less refractory chemistries, especially mineral chemistries of spinels, exhibited by Lanzarote mantle xenoliths with porphyroclastic textures are not representative of the chemistries of their source mantle reservoir, but are the result of interaction between peridotite and melt. Mineral chemistries of the dunites rule out any petrogenetic relation between their source and the harzburgite xenolith source. Crustal samples represent low-pressure cumulates from the Jurassic-age oceanic crust underlying Lanzarote.

APPENDIX

Table A1: GPS locations and had sample descriptions

Sample	Locality	Longitude	Latitude	Hand sample Description[1,2]
LZ06-02A	Caldera de Los Cuervos	13°41.345'	28°59.317'	Small Harzburgite, thin dark selvage, melt infiltration
LZ06-02B	Calder de Los Cuervos	13°41.345'	28 59 317	Small Harzburgite, thin dark selvage
LZ06-03i	Calder de Los Cuervos	13°41.515'	28°59.509'	Small Harzburgite, thick dark selvage
LZ06-04A	Pico Partido	13°43.092'	29°00.365'	Small Harzburgite, thin dark selvage
LZ06-04B	Pico Partido	13°43.092'	29°00.365'	Medium Harzburgite, thick dark selvage
LZ06-04C	Pico Partido	13°43.092'	29°00.365'	Medium Harzburgite, thin dark selvage
LZ06-04D	Pico Partido	13°43.092'	29°00.365'	Small Harzburgite, thick dark selvage
LZ06-05	Montana De La Nuces	13°41.012'	29°00.220'	Medium Harzburgite, no selvage, iddingzitized surface olivines
LZ1001A	Caldera de Los Cuervos	13°41.580'	28°59.523'	Medium Harzburgite, thick vesicular selvage, melt interaction
LZ1001B	Caldera de Los Cuervos	13°41.580'	28°59.523'	Medium Harzburgite, thick vesicular selvage
LZ1002	Pico Partido	13°43.083'	29°00.693'	Medium Harzburgite, thin dark selvage
LZ1003A	Pico Partido	13°43.086'	29°00.698'	Large Harzburgite, thick gark selvage
LZ1003B	Pico Partido	13°43.086'	29°00.698'	Medium Harzburgite, thin dark selvage
LZ1003C	Pico Partido	13°43.086'	29°00.698'	Medium Harzburgite, most of xenolith exposed
LZ1004A	Pico Partido	13°43.080'	29°00.683'	Medium Harzburite, thin dark selvage
LZ1004B	Pico Partido	13°43.080'	29°00.683'	Small Harzburgite thin oxidized selvage
LZ1005	Pico Partido	13°43.109'	29°00.797'	Large Harzburgite, thin brown selvage
LZ1006	El Golfo Maar	13°49.872'	28°58.481'	Small Harzburgite, thin dark selvage
LZ1007	El Cuchillo	13°39.447'	29°05.251'	Small Harzburgite, thin oxidized selvage, interior oxidized
LZ1008	El Cuchillo	13°39.436'	29°05.249'	Small Lherzolite, thin oxidized selvage, interior oxidized
LZ1009	El Cuchillo	13°39.420'	29°05.244'	Small round Harzburgite, thin oxidized selvage, interior oxidized
LZ10010	El Cuchillo	13°39.442'	29°05.250'	Small Harzburgite, thin oxidized selvage, interior oxidized
LZ1011	El Cuchillo	13°39.484'	29°05.277'	Small Harzburgite, thin oxidized selvage, interior oxidized
LZ1012A	El Cuchillo	13°39.492'	29°05.275'	Small Lherzolite, thin oxidized selvage, interior oxidized
LZ1012B	El Cuchillo	13°39.492'	29°05.275'	Small Harzburgite, thin oxidized selvage, interior oxidized
LZ1013A	El Cuchillo	13°39.499'	29°05.279'	Small Gabbro, thick vesicular selvage, oxidized interior
LZ1014	El Cuchillo	13°39.510'	29°05.288'	Small Lherzolite, thin oxidized selvage, interior oxidized, cpx vein
LZ1015Ai	Guatiza	13°27.884'	29°04.646'	Small crustal xenolith, thin oxidized selvage, crosscutting veins
LZ1015Aii	Guatiza	13°27.884'	29°04.646'	Small Gabbro, thin oxidized selvage, iddinsitized olivines
LZ1015B	Guatiza	13°27.884'	29°04.646'	Small Gabbro, thin oxidized selvage
LZ1016A	Guatiza	13°27.888'	29°04.674'	Medium Gabbro, thin oxidized selvage, interior oxidized
LZ1016B	Guatiza	13°27.888'	29°04.674'	Small Harzburgite, thin oxidized vesicular selvage
LZ1016C	Guatiza	13°27.888'	29°04.674'	Small plagioclase-lherzolite, no selvage
LZ1016D	Guatiza	13°27.888'	29°04.674'	Small Dunite, altered, no selvage
LZ1016E	Guatiza	13°27.888'	29°04.674'	Small Dunite, thin oxidized selvage, large spinels
LZ1016F	Guatiza	13°27.888'	29°04.674'	Small Harzburgite, thick oxidized vesicular selvage

Table A1: Continued

Sample	Locality	Longitude	Latitude	Handsample Description[1,2]
LZ1016Gi	Guatiza	13°27.888'	29°04.674'	Small Gabbro, thick oxidized selvage
LZ1016Gii	Guatiza	13°27.888'	29°04.674'	Small Dunite, thin oxidized selvage, large spinels
LZ1016Hi	Guatiza	13°27.888'	29°04.674'	Small Dunite, no selvage, large spinels
LZ1016Hii	Guatiza	13°27.888'	29°04.674'	Small Dunite, thick oxidized selvage, interior oxidized
LZ1016I	Guatiza	13°27.888'	29°04.674'	Small Harzburgite, no selvage
LZ1017A	Montana De La Nuces	13°41.003'	29°00.367'	Very large Harzburgite (20+cm), thin brown selvage
LZ1017B	Montana De La Nuces	13°41.003'	29°00.367'	Large Harzburgite, thin brown selvage
LZ1201	Montana Colorada	13°40.945'	29°0.402'	Large Calc-Silicate Xenolith
LZ1202	Montana Colorada	13°40.937'	29°0.397'	Large Harzburgite
LZ1203A	Montana Colorada	13°40.940'	29°0.338'	Large Altered Harzburgite
LZ1203B	Montana Colorada	13°40.940'	29°0.338'	Large Harzburgite
LZ1203C	Montana Colorada	13°40.940'	29°0.338'	Small Hydrothermally altered basalt
LZ1203D	Montana Colorada	13°40.940'	29°0.338'	Small Altered Harzburgite and crustal xenoliths
LZ1204	El Cuchillo	13°38.812'	29°5.258'	Medium Lherzolite
LZ1204B	El Cuchillo	13°38.812'	29°5.258'	Large Harzburgite
LZ1205	El Cuchillo	13°38.812'	29°5.360'	Small Lherzolite with cpx veins
LZ1206A	Guatiza South	13° 29.244'	29° 3.720'	Small Harzburgite
LZ1206B	Guatiza South	13° 29.244'	29° 3.720'	Medium Harzburgite with chromite veins
LZ1206C	Guatiza South	13° 29.244'	29° 3.720'	Large Harzburgite
LZ1206D	Guatiza South	13° 29.244'	29° 3.720'	Dunite with carbonate vein
LZ1207A	Pico Partido	13°43.146'	29°0.485'	Large Harzburgite
LZ1207B	Pico Partido	13°43.146'	29°0.485'	Large flat Gabbro
LZ1207C	Pico Partido	13°43.146'	29°0.485'	Deformed Harzburgite
LZ1207D	Pico Partido	13°43.146'	29°0.485'	Medium Gabbro
LZ1207E	Pico Partido	13°43.146'	29°0.485'	Medium serpentinized xenolith
LZ1208A	Pico Partido	13°42.952'	29°0.637'	Large Harzburgite, extensive melt interaction
LZ1208B	Pico Partido	13°42.952'	29°0.637'	Small Pyroxenite
LZ1208C	Pico Partido	13°42.952'	29°0.637'	Large Altered Dunite
LZ1208D	Pico Partido	13°42.952'	29°0.637'	Medium Harzburgite with chromite vein
LZ1208E	Pico Partido	13°42.952'	29°0.637'	Large Hydrothermally altered basalt
LZ1209A	El Golfo Maar	13°49.871'	28°58.474'	Small Harzburgite
LZ1209B	El Golfo Maar	13°49.871'	28°58.474'	Small Harzburgite
LZ1209C	El Golfo Maar	13°49.871'	28°58.474'	Large Harzburgite
LZ1210	El Golfo Maar	13°49.871'	28°58.474'	Small Harzburgite
LZ1211	El Golfo Maar	13°49.871'	28°58.474'	Small Harzburgite

[1]Large: greater than 10 cm across

Medium: between about 6 and 10 cm across

Small; less than about 6 cm across

[2]For LZ12* samples, only brief field descriptions are given

Table A2: Whole rock major element data (wt.%)

Sample	LZ0602B	LZ0603i	LZ0604A	LZ0604B	LZ0604C	LZ0604D	LZ0605	LZ1001A	LZ1001B
Locality[1]	3	3	2	2	2	2	4	3	3
Rock Type[2]	1	1	1	1	1	1	1	1	1
SiO_2	43.81	44.04	43.03	42.44	43.63	42.59	43.52	44.01	41.63
TiO_2	0.02	0.04	0.03	0.05	0.03	0.07	0.03	0.02	0.01
Al_2O_3	0.74	1.2	0.97	0.76	0.84	1.21	0.75	1.15	0.8
$Fe_2O_3^T$	8.64	8.31	9.13	8.71	8.43	8.91	8.8	8.43	8.72
MnO	0.14	0.13	0.14	0.14	0.15	0.14	0.14	0.14	0.15
MgO	45.88	45.08	45.2	46.65	45.37	45.4	45.45	44.41	46.51
CaO	0.44	0.76	0.69	0.53	0.38	0.78	0.58	0.7	0.53
Na_2O	0.12	0.04	0.03	0.04	0.11	0.06	0.02	0.16	0.14
K_2O	0.01	0.002	0	0	0.05	0.005	0	0.024	0.01
P_2O_5	0.04	0.03	0.02	0.03	0.03	0.03	0.02	0.018	0.007
Mg-no.	84.2	84.4	83.2	84.3	84.3	83.6	83.8	84.0	84.2
Sample	LZ1002	LZ1003A	LZ1003B	LZ1003C	LZ1004A	LZ1004B	LZ1005	LZ1006	LZ1007
Locality[1]	2	2	2	2	2	2	2	1	5
Rock Type[2]	1	1	1	1	1	1	1	1	1
SiO_2	42.45	43.71	44.04	43.55	43.2	43.59	43.41	43.15	41.64
TiO_2	0.02	0.03	0.02	0.03	0.02	0.02	0.01	0.02	0.02
Al_2O_3	0.68	0.91	1.24	1.1	0.78	1.05	0.83	0.83	0.68
$Fe_2O_3^T$	8.79	8.31	8.57	8.75	8.74	8.72	8.43	8.79	9.48
MnO	0.14	0.13	0.14	0.14	0.14	0.14	0.17	0.14	0.14
MgO	46.26	45.06	44.07	44.42	45.28	44.61	45.17	45.57	45.96
CaO	0.55	0.67	0.99	0.98	0.68	0.86	0.66	0.39	0.56
Na_2O	0.06	0.19	0.04	0.08	0.16	0.08	0.17	0.1	0.11
K_2O	0	0.034	0	0.007	0.018	0	0.007	0.026	0.021
P_2O_5	0.004	0.006	0.005	0.007	0.014	0.002	0.003	0.005	0.012
Mg-no.	84.0	84.4	83.7	83.5	83.8	83.6	84.3	83.8	82.9

[1] Localities– 1= El Gulfo Maar; 2=Pico Partido; 3= Caldera de Los Cuervos; 4=Montana de Las Nueces 5=El Cuchillo Maar: 6=Guatiza

[2] Rock Types– 1=Harzburgite; 2=Lherzolite; 3=Dunite; 4=Gabbro; 5=Troctolite 6=Plagioclase-Lherzolite

Table A2: Continued

Sample	LZ1008	LZ1009	LZ10010	LZ1011	LZ1012A	LZ1012B	LZ1013A	LZ1014	LZ1015Ai
Locality[1]	5	5	5	5	5	5	5	5	6
Rock Type[2]	2	1	1	1	2	1	4	2	5
SiO_2	42.17	41.96	42.22	43.1	42.98	42.6	47.61	42.79	43.48
TiO_2	0.07	0.08	0.02	0.08	0.07	0.02	0.12	0.14	0.2
Al_2O_3	0.7	0.76	0.73	0.72	1.19	0.73	22.52	1.27	19.82
$Fe_2O_3^T$	10.14	12.45	8.89	9.34	8.83	8.58	4.03	9.01	6.12
MnO	0.17	0.25	0.14	0.2	0.14	0.13	0.08	0.15	0.09
MgO	44.42	42.6	46.28	44.59	44.49	45.85	8.02	42.68	17.78
CaO	1.28	0.84	0.49	0.85	1.04	0.8	15.5	2.33	10.75
Na_2O	0.14	0.13	0.09	0.14	0.12	0.06	1.76	0.27	1.2
K_2O	0.021	0.024	0.012	0.04	0.011	0	0.144	0.053	0.106
P_2O_5	0.027	0.021	0.007	0.029	0.018	0.005	0.01	0.035	0.061
Mg-no.	81.4	77.4	83.9	82.7	83.4	84.2	66.6	82.6	74.4

Sample	LZ1015Aii	LZ1015Bi	LZ1016A	LZ1016B	LZ1016C	LZ1016Di	LZ1016E	LZ1016F	LZ1016Gi
Locality[1]	6	6	6	6	6	6	6	6	6
Rock Type[2]	4	4	4	1	6	3	3	1	4
SiO_2	49.41	47.24	48.43	42.25	42.89	38.17	39.21	43.75	48.38
TiO_2	0.12	0.13	0.15	0.06	0.11	0.04	0.14	0.01	0.14
Al_2O_3	14.34	14.37	10.62	0.86	4.67	0.72	2	0.64	18.36
$Fe_2O_3^T$	5.09	4.47	5.78	8.66	8.09	11.77	10.54	8.3	3.8
MnO	0.12	0.09	0.11	0.14	0.15	0.18	0.17	0.14	0.07
MgO	12.65	15.06	18.32	45.83	35.15	47.19	45.02	45.76	9.19
CaO	16.67	16.87	16.05	0.58	7.75	0.33	0.97	0.57	19.13
Na_2O	0.99	0.79	0.51	0.12	0.26	0.04	0.19	0.02	0.82
K_2O	0.003	0.051	0.003	0.05	0.017	0.011	0.093	0	0.052
P_2O_5	0.013	0.014	0.013	0.027	0.037	0.034	0.053	0.015	0.031
Mg-no.	71.3	77.1	76.0	84.1	81.3	80.0	81.0	84.6	70.7

[1] Localities– 1= El Gulfo Maar; 2=Pico Partido; 3= Caldera de Los Cuervos; 4=Montana de Las Nueces 5=El Cuchillo Maar: 6=Guatiza

[2] Rock Types– 1=Harzburgite; 2=Lherzolite; 3=Dunite; 4=Gabbro; 5=Troctolite 6=Plagioclase-Lherzolite

Table A2: Continued

Sample	LZ1016Gii	LZ1016Hi	LZ1016Hii	LZ1016I	LZ1017A	LZ1017B	LZ0602A
Locality[1]	6	6	6	6	4	4	3
Rock Type[2]	3	3	3	1	1	1	1
SiO_2	38.57	38.46	39.47	41.91	42.71	42.98	42.83
TiO_2	0.06	0.07	0.15	0.07	0.02	0.01	0.02
Al_2O_3	1.28	1.46	3.22	0.72	0.7	0.66	0.83
$Fe_2O_3^T$	11.57	11.59	11.29	9.02	8.54	8.66	8.66
MnO	0.17	0.18	0.19	0.14	0.13	0.13	0.13
MgO	46.07	46.64	42.42	45.71	45.95	45.97	46.75
CaO	0.43	0.37	1.73	0.87	0.54	0.53	0.4
Na_2O	0.08	0.05	0.27	0.15	0.04	0.03	0.07
K_2O	0.019	0.005	0.087	0.066	0	0	0.004
P_2O_5	0.021	0.026	0.061	0.013	0.002	0.002	0.03
Mg-no.	79.9	80.1	79.0	83.5	84.3	84.1	84.4

[1]Localities– 1= El Gulfo Maar; 2=Pico Partido; 3= Caldera de Los Cuervos; 4=Montana de Las Nueces 5=El Cuchillo Maar: 6=Guatiza

[2]Rock Types– 1=Harzburgite; 2=Lherzolite; 3=Dunite; 4=Gabbro; 5=Troctolite 6=Plagioclase-Lherzolite

Table A3: Whole rock trace element abundances (ppm)

Specimen	LZ06-02A	LZ06-02B	LZ06-03i	LZ06-04A	LZ06-04B	LZ06-04C	LZ06-04D	LZ06-05	LZ1001A
Rock Type	1	1	1	1	1	1	1	1	1
Rb	0.9	0.6	<0.5	0.9	1	0.7	<0.5	<0.5	<0.5
Sr	26	49	37	12	13	19	20	8	28
Y	<0.5	0.5	-	<0.5	<0.5	-	-	<0.5	0.9
Zr	10	12	15	12	10	15	18	11	7
V	26	27	27	25	18	29	34	30	23
Ni	2663	2509	2385	2563	2735	2550	3020	2415	2262
Cr	2745	1910	2618	2410	1865	3375	2125	2990	3484
Nb	2.3	3	-	1.7	2	-	-	1.7	0.9
Ga	<0.5	<0.5	-	<0.5	<0.5	-	-	<0.5	1.3
Cu	3	5	-	5	2	-	-	6	3
Zn	43	43	-	45	44	-	-	50	49
Co	110	117	112	122	109	114	130	116	103
Ba	3	6	-	12	4	-	-	12	27
La	1	<1	-	<1	<1	-	-	<1	1
Ce	1	3	-	<1	<1	-	-	<1	2
U	<0.5	<0.5	-	<0.5	<0.5	-	-	<0.5	<0.5
Th	0.9	<0.5	-	<0.5	<0.5	-	-	0.6	<0.5
Sc	8	8	-	6	5	-	-	10	8
Pb	7	6	-	7	6	-	-	5	1

Specimen	LZ1001B	LZ1002	LZ1003A	LZ1003B	LZ1003C	LZ1004A	LZ1004B	LZ1005	LZ1006
Rock Type	1	1	1	1	1	1	1	1	1
Rb	<0.5	<0.5	<0.5	0.5	<0.5	<0.5	0.5	1.7	<0.5
Sr	15	2	12	6	9	25	6	12	10
Y	1.2	<0.5	0.9	<0.5	0.8	1.8	0.8	1.1	<0.5
Zr	8	8	8	9	9	8	9	8	9
V	23	20	21	26	32	23	30	18	16
Ni	2427	2486	2287	2295	2276	2396	2310	2364	2258
Cr	3108	2798	2725	2345	3004	2960	3110	2604	1940
Nb	<0.5	<0.5	<0.5	<0.5	<0.5	<0.5	<5	<0.5	<0.5
Ga	1	0.5	0.9	0.8	1.2	1.4	0.9	0.9	1
Cu	5	4	5	2	6	5	3	3	3
Zn	46	47	41	43	45	45	46	52	41
Co	107	118	102	110	105	108	110	112	100
Ba	10	4	19	10	4	36	4	122	3
La	<1	<1	1	<1	1	<1	1	<1	1
Ce	2	4	1	1	3	2	<1	3	2
U	<0.5	<0.5	<0.5	<0.5	<0.5	<0.5	<0.5	<0.5	<0.5
Th	<0.5	<0.5	<0.5	<0.5	<0.5	<0.5	<0.5	<0.5	<0.5
Sc	5	4	7	6	7	6	8	4	7
Pb	<1	<1	1	<1	1	<1	<1	1	<1

[2]Rock Types– 1=Harzburgite; 2=Lherzolite; 3=Dunite; 4=Gabbro; 5=Troctolite; 6=Plagioclase-Lherzolite

Table A3: Continued

Specimen	LZ1007	LZ1008	LZ1009	LZ1010	LZ1011	LZ1012A	LZ1012B	LZ1013A	LZ1014
Rock Type	1	2	1	1	1	1	1	4	1
Rb	<0.5	<0.5	<0.5	<0.5	<0.5	0.8	<0.5	2.5	<0.5
Sr	27	24	12	12	52	11	9	804	55
Y	1	2.6	0.9	<0.5	1.1	0.5	<0.5	1.9	3
Zr	9	4	2	8	9	5	9	24	9
V	29	23	50	31	57	38	29	71	44
Ni	2364	2192	2052	2457	2101	2341	2414	143	2071
Cr	2863	2160	2242	1738	2924	1981	2214	303	2466
Nb	<0.5	<0.5	0.7	<0.5	2.1	<0.5	<0.5	<0.5	0.5
Ga	0.9	1.1	1.9	1.1	2	2.2	2.7	11.2	2.2
Cu	4	3	4	6	6	4	5	62	13
Zn	48	65	142	43	78	48	42	22	52
Co	111	113	118	106	96	112	107	21	94
Ba	7	15	2	15	42	5	16	75	37
La	<1	<1	<1	2	4	<1	1	7	3
Ce	1	3	<1	2	8	3	<1	10	8
U	<0.5	,0.5	<0.5	<0.5	<0.5	<0.5	<0.5	1.5	<0.5
Th	<0.5	<0.5	<0.5	<0.5	<0.5	<0.5	<0.5	0.5	<0.5
Sc	7	6	6	5	8	5	6	27	11
Pb	<1	<1	<1	<1	<1	<1	<1	<1	<1

Specimen	LZ1015Ai	LZ1015Aii	LZ1015B	LZ1016A	LZ1016B	LZ1016C	LZ1016D	LZ1016E	LZ1016F
Rock Type	5	4	4	4	1	5	1	1	1
Rb	3.3	<0.5	1	0.5	1.3	<0.5	<0.5	1.9	<0.5
Sr	107	34	55	23	16	23	5	29	3
Y	2	4.7	4.1	6.1	<0.5	2.7	1.1	4.7	<0.5
Zr	20	12	13	13	7	8	9	6	9
V	36	133	103	117	25	63	21	38	21
Ni	413	165	274	307	2436	1019	1837	2530	2393
Cr	104	687	940	1020	3063	1979	5546	5709	2070
Nb	1.9	<0.5	<0.5	<0.5	<0.5	<0.5	<0.5	0.9	<0.5
Ga	9	8.2	6.9	6.2	0.9	4.2	1.3	2.4	0.8
Cu	16	6	17	16	12	5	11	9	7
Zn	40	23	22	28	50	37	60	56	42
Co	61	29	32	42	118	117	148	115	103
Ba	149	<2	135	32	304	148	23	415	58
La	7	6	9	7	<1	1	1	<1	1
Ce	17	10	15	15	5	5	<1	<1	<1
U	<0.5	0.5	<0.5	<0.5	<0.5	<0.5	<0.5	<0.5	<0.5
Th	<0.5	0.5	<0.5	<0.5	<0.5	<0.5	<0.5	<0.5	<0.5
Sc	13	44	38	40	6	21	8	7	8
Pb	<1	<1	<1	<1	<1	<1	<1	2	<1

[2]Rock Types– 1=Harzburgite; 2=Lherzolite; 3=Dunite; 4=Gabbro; 5=Troctolite; 6=Plagioclase-Lherzolite

Table A3: Continued

Specimen	LZ1016Gi	LZ1016Gii	LZ1016Hi	LZ1016Hii	LZ1016I	LZ1017A	LZ1017B
Rock Type	**4**	**3**	**1**	**1**	**1**	**1**	**1**
Rb	1.3	<0.5	<0.5	1.5	0.5	<0.5	<0.5
Sr	137	14	7	33	17	2	1
Y	2.9	1.2	<0.5	3.4	<0.5	<0.5	<0.5
Zr	16	10	9	5	9	9	9
V	135	34	36	37	26	19	21
Ni	105	1846	2130	2128	2392	2425	2463
Cr	446	6598	8611	3170	2561	3009	2316
Nb	<0.5	<0.5	<0.5	1.3	<0.5	<0.5	<0.5
Ga	9.7	1.8	0.8	<0.5	2.2	<0.5	<0.5
Cu	9	8	3	10	4	4	4
Zn	19	60	56	58	43	45	44
Co	16	143	137	124	101	112	114
Ba	112	224	46	184	241	<2	6
La	7	2	1	<1	2	<1	<1
Ce	13	<1	<1	5	<1	1	5
U	<0.5	<0.5	<0.5	<0.5	<0.5	<0.5	<0.5
Th	<0.5	<0.5	<0.5	<0.5	<0.5	<0.5	<0.5
Sc	43	7	7	6	8	6	5
Pb	<1	<1	<1	<1	2	2	<1

[2]Rock Types– 1=Harzburgite; 2=Lherzolite; 3=Dunite; 4=Gabbro; 5=Troctolite; 6=Plagioclase-Lherzolite

Procedures for determining Modal Percentages

Scanning in Slides

-Turn on Cannon Scanner

-Remove top protective sheet.

-Set film guide on glass.

-Open Cannon MP Navigator EX 3.1

-Choose "Scan/Import" icon on top left

-Select "Film" in left margin

-Click "Specify Settings"

-Set "Film Type" to "Auto," "Document Size" will be "35mm film" and set "Scanning Resolution" to the highest dpi (4800dpi).

-Press OK

-Check the box that says Use Scanner Driver. "Scan" button will change to "Open Scanner Driver," press this button.

-With one sheet of polarizing film against the glass in the film guide, place slide on top of the piece of polarizing film.

-Close cover and Press Preview. You will then need to change the selection box on the preview so that it includes your entire slide

-Once this is done, press the "Scan" button.

-After scanning is complete, you have an option to scan more images.

-To get a cross-polarized image of your scan, place a second piece of polarizing film on TOP of your slide so the slide is sandwiched between two oppositely oriented polarizing sheets, then close lid and scan.

-After finishing scans, exit Scanner Driver. Cannon MP Navigator EX 3.1 window will remain open with all scanned images.

-Save each of these images individually as their sample names in a folder with nothing else in it.

-Using an editing program (i.e., Corel Draw or Photoshop), erase all parts of the image that aren't sample, this includes of course the area surrounding the slide, and also the

edges of your sample that have holes, selvage, tears, etc. This step is very important, so you need to be thorough. Make sure that the eraser tool you are using has a sharp, clean edge (i.e.. 100% "hardness" in Photoshop). Save the edited version as a pdf.

Using ImageJ

-Open the ImageJ program.

-Go to File menu

-Select "Open" and choose the file you wish to do modal analysis on.

-Next, to convert your image to greyscale, go into the Image menu

- Select the Type menu.

-Choose 32-bit.

-Now open the Image menu

- Select the Adjust menu

-Select Threshold

-Set the lower bound all the way to the lowest number (all the way to the left), and set the upper bound where the red selected area takes up all of your sample area, but not the surrounding white part of the image. This should be very obvious. DO NOT SELECT "SET," the measurements can be made without doing so and this way you won't have to keep re-opening your image, but instead can make continuous measurements.

-Go into the Analyze menu

Select Measure.

-A Results window will pop up. Record the total pixels, "Area," and record the %Area. The Min and Max in the Results window are NOT the thresholds you've chosen but the total for the entire image and these won't be very helpful. You have to record your minimum and maximum threshold values for each measurement directly from the Threshold window.

-You have now recorded the values for the whole slide, and can begin targeting specific mineral phases. It is best to start from the very lowest values and work your way up through the different mineral phases. For example, a dark mineral (in PPL)

like spinel would be at low values, so start with both the upper and lower bounds all the way to the left, and move the upper bound until you feel that all of the darkest mineral phase is selected in red, without overlapping another, lighter mineral phase. Measure again, record %Area from Results window, and threshold values from Threshold window

-Since there is some room for error here, you will want to do some sort of extra measurements to see how much a slight change in threshold will change your values. One way to do this is to do two more calculations for each mineral phase: an extended range and a narrowed range, recording the threshold values and %Area for each.

-Do this for each consecutively lighter mineral phases. You will need to match the upper and lower thresholds from the mineral phase above, and below the targeted phase. This will assure that the %Areas add up to the full area of the sample being analyzed.

-An example of an excel worksheet setup to record all of this data might look something like this:

(Sample)

	Pixels	%	% real	Est. uncer.	Threshold min-max
Total area	(RW)				
Area of slide		(RW)			(TW)
Mineral Phase 1		(RW)	**C**	**C**	(TW)
*extended		(RW)	**C**	**C**	(TW)
*narrowed		(RW)	**C**	**C**	(TW)
Mineral Phase 2		(RW)	**C**	**C**	(TW)
*extended		(RW)	**C**	**C**	(TW)
*narrowed		(RW)	**C**	**C**	(TW)
Mineral Phase 3		(RW)	**C**	**C**	(TW)
*extended		(RW)	**C**	**C**	(TW)
*narrowed		(RW)	**C**	**C**	(TW)
Mineral Phase 4		(RW)	**C**	**C**	(TW)
*extended		(RW)	**C**	**C**	(TW)
*narrowed		(RW)	**C**	**C**	(TW)

(RW)=from results window, (TW)=from threshold window, C=calculated in spreadsheet

-When you are finished with your analysis of your first sample, you can close the image, threshold, and results window. You do not need to save the results or the changes to the image. To continue analyzing further samples you can select "Open Next" before closing the image window IF all of your images are saved together in a folder with no other files between them.

-Recalculate the percent area to the area of the slide (%from analysis/%Area of slide). A good check to make sure your thresholds didn't overlap or miss any values is to add up the %real for all the mineral phases (dark orange). This should add up to 100 (or within .1 of 100 due to rounding).

-Here is an example of olivine thresholds selected for sample LZ1001B, the results of the measurement made from this threshold choice would go in the '*extended' row of the chart below.

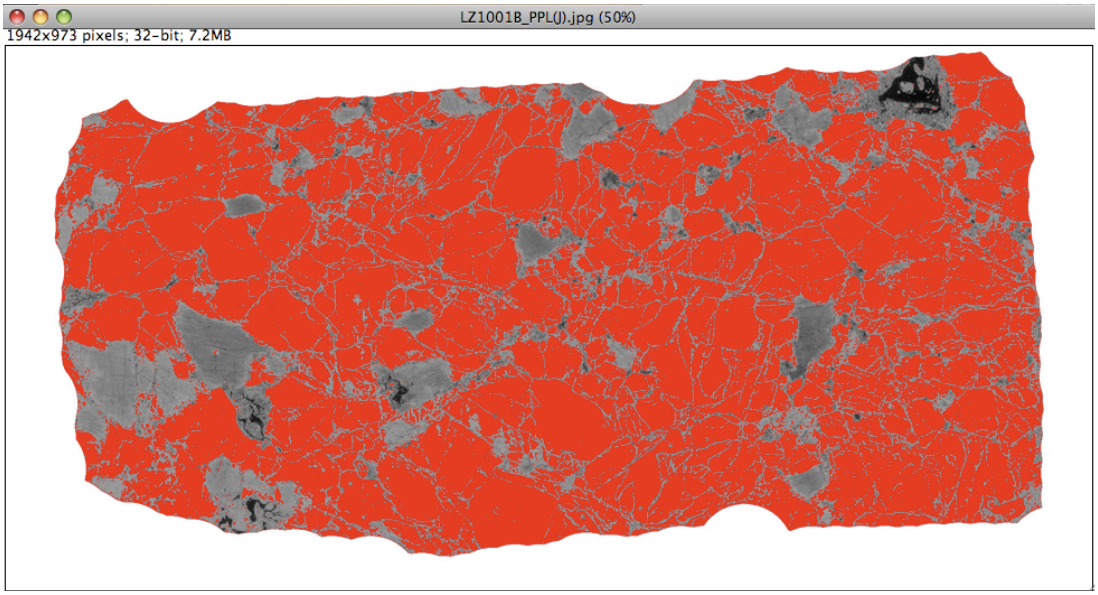

LZ1001B					
	Pixels	%	% real	Est uncer.	Threshold min-max
Total area	1889566				
Area of slide		71.848			13-200.91
Olivine		51.399	**71.539**		149.66-200.91
*extended					
*narrowed		48.121	**66.976**		152.51-200.91
Opx		19.674	**27.383**		87.97-149.66
*extended		22.952	**31.945**		87.02-152.51
*narrowed		16.778	**23.352**		89.87-146.81
Spinel		0.557	**0.775**		13-78.48
*extended		0.614	**0.855**		13-81.33
*narrowed		0.496	**0.690**		13-74.69
Neoblasts		0.218	**0.303**		78.48-87.97
*extended		0.351	**0.489**		74.69-89.87
*narrowed		0.139	**0.193**		82.28-87.02

REFERENCES

Abdel-Monem, A., Watkins, N.D., Gast, P.W. (1972) Potassium-argon ages, volcanic stratigraphy, and geomagnetic polarity history of the Canary Islands: Tenerife, La Palma and El Hierro. *American Journal of Science*, **272**, 805-825.

Abu El-Rus, M.A., Neumann, E.-R., Peters, V. (2006) Serpentinization and dehydration in the upper mantle beneath Fuerteventura (eastern Canary Islands): evidence from mantle xenoliths. *Lithos,* **89**, 24-46.

Anguita F., Hernan F. (1975) A Propagating Fracture Model Versus A Hot Spot Origin For The Canary Islands. *Earth and Planetary Science Letters,* **27**, 11-19.

Anguita F., Hernan F., (2000) The Canary Islands origin: a unifying model. *Journal of Volcanology and Geothermal Research,* **103**, 1-26.

Arai S. (1994) Characterization of peridotites by olivine-spinel compositional relationship: Review and interpretation. *Chemical Geology,* **113**, 191-204.

Barnes S.J., Naldrett A.J., Gorton M.P. (1985) The origin of the fractionation of platinum-group elements in terrestrial magmas. *Chemical Geology,* **53**, 303–323.

Bodinier J.L., Godard M. (2003) Orogenic, ophiolitic, and Abyssal Peridotites. *Treatise on Geochemistry,* **2: The Mantle and Core**, 1-73.

Boyet M., Carlson R.W. (2005) ^{142}Nd Evidence for Early Earth (>4.53 Ga) Global Differentiation of the Silicate Earth. *Science* **309**, 576-581.

Caro G., Bourdon B., Birck J.L., Moorbath S. (2003) ^{146}Sm–^{142}Nd evidence from Isua metamorphosed sediments for early differentiation of Earth's mantle. *Nature* **423**, 428-432.

Carracedo J.C., Badiola E.R., Soler V. (1992) 1730-1736 eruption of Lanzarote, Canary Islands: a long, high magnitude basaltic fissure eruption. *Journal of Volcanology and Geothermal Research,* **53**, 239-250.

Carracedo J.C., Day S., Guillou H., Badiola E.R., Canas JA, Pérez F.J. (1998) Hotspot Volcanism Close to a Passive Continental Margin: the Canary Islands. *Geological Magazine,* **135**, 591-604.

Carracedo, J.-C., Rodríguez Badiola, E., Guillou, H., De La Nuez, J. & Perez Torrado, F.J. (2001) Geology and volcanology of La Palma and El Hierro (Canary Islands). *Estudios Geologicos*, **57**, 175-273.

Carracedo J.C., Day S. (2002) Canary Islands; Classical Geology in Europe 4: Terra Publishing, Edinburgh Scotland. 294 pp.

Carracedo, J.C., Pérez-Torrado, F. J., Ancochea, E., Meco, J., Hernán, F., Cubas, C. R., Casillas, R., Badiola, E. R. & Ahijado A. (2002) Cenozoic volcanism II: the Canary Islands. In: Gibbons, W. & Moreno, T. (Eds.) *The Geology of Spain*. Geological Society, London, pp. 439-472.

Creaser, R.A., Papanastassiou, D.A., Wasserburg, G.J. (1991) Negative thermal ion mass spectrometry of osmium, rhenium, and iridium. *Geochimica et Cosmochimica Acta,* **55**, 397-401.

Coltorti, M., Bonadiman, C., O'Reilly, S.Y., Griffin, W.L., Pearson, N.J. (2010) Buoyant ancient continental mantle embedded in oceanic lithosphere (Sal Island, Cape Verde Archipelago). *Lithos,* **120,** 223-233.

Day J.M.D., Pearson D.G., Macpherson C.G., Lowry D., Carracedo J.C. (2010) Evidence for distinct proportions of subducted oceanic crust and lithosphere in HIMU type mantle beneath El Hierro and La Palma, Canary Islands. *Geochimica et Cosmochimica Acta,* **74,** 6565-6589.

Day J.M.D., Walker R.J., Hilton D.R., Carracedo J.-C., Hanski E. (2008) Constraining deep mantle contributions to Canary Island lavas. Geochimica et Cosmochimica Acta, 72, A204.

Day J.M.D., Walker R.J., Qin, L., Rumble D. (2012) Late accretion as a natural consequence of planetary growth. *Nature Geoscience*, **5**, 614-617.

Frezzotti, M.-L., Touret, J.L.R., Lustenhouwer, W.J., Neumann, E.-R. (1994) Melt and fluid inclusions in dunite xenoliths from La Gomera, Canary Islands: tracking the mantle metasomatic fluids. *European Journal of Mineralogy,* **6**, 805-817.

Frezzotti, M.-L., Touret, J.L.R., Neumann, E.-R. (2002a) Ephemeral carbonate melts in the upper mantle: carbonate-silicate immiscibility in microveins and inclusions within spinel peridotite xenoliths, La Gomera, Canary Islands. *European Journal of Mineralogy,* **14**, 891-904.

Frezzotti, M.-L., Andersen, T., Neumann, E.-R., Simonsen, S.L. (2002b) Carbonatite melt-CO2 fluid inclusions in mantle xenoliths from Tenerife, Canary Islands: a story of trapping, immiscibility and fluid-rock interaction in the upper mantle. *Lithos,* **64**, 77-96.

Fuster J.M., Fernandez S., Sagredo J. (1968) Geologia y Volcanologia de las Islas Canarias: Lanzarote. Instituto Lucas Mallada, Madrid.

Guillou H., Carracedo J.C., Perez F.J., Badiola E.R. (1996) K–Ar ages and magnetic stratigraphy of a hotspot induced, fast grown oceanic island: El Hierro, Canary Islands. *Journal of Volcanology and Geothermal Research,* **73**, 141-155.

Guillou H., Carracedo J.C., Day S.J. (1998) Dating of the Upper Pleistocene–Holocene volcanic activity of La Palma using the unspiked K–Ar technique. *Journal of Volcanology and Geothermal Research* **86**, 137-149.

Hilton, D.R., Day, J.M.D., Hamn, D., Carracedo, J.-C. (2008) Volatile systematics of the Canary Islands hotspot. *Geochimica et Cosmochimica Acta,* **72**, A378.

Hofmann A.W. (1997) Mantle geochemistry: the message from oceanic volcanism. *Nature,* **385**, 219-229.

Hofmann, A.W. (2003) Sampling mantle heterogeneity through oceanic basalts: isotopes and trace elements. In: *The Mantle* (Ed. Carlson, R.W.) **Vol. 2**, Treatise on Geochemistry (Eds. Holland, H.D. and Turekian, K.K.), Elsevier-Pergamon, Oxford, pp. 61-101 (2003).

Horn I., Foley S.F., Jackson S.E., Jenner G.A. (1994) Experimentally determined partitioning of high-field strength and selected transition elements between spinel and basaltic melts. *Chemical Geology,* **117**, 193-218.

Jaques A, Green D. (1980) Anhydrous Melting of Peridotite at 0-15 Kb Pressure and the Genesis of Tholeiitic Basalts. *Contributions to Mineralogy and Petrology,* **73**, 287-310.

Kennedy A.K., Lofgren G.E., Wasserburg GJ (1993) An experimental study of trace element partitioning between olivine, orthopyroxene and melt in chondrules: equilibrium values and kinetic effects. *Earth and Planetary Science Letters,* **115**, 177-195.

Klugel A. (1998) Reactions between mantle xenoliths and host magma beneath La Palma (Canary Islands): constraints on magma ascent rates and crustal reservoirs. *Contributions to Mineralogy and Petrology,* **131**, 237-257.

Lindsley D.H., Dixon SA (1996) Diopside–Enstatite Equilibria at 850º to1400ºC, 5 to 35 KB. *American Journal of Science,* **276**, 1285-1301.

Malamud, B.D., Turcotte, D.L. (1999) How many plumes are there? *Earth and Planetary Science Letters*, **174**, 113-124.

Marinoni L., Pasquare G. (1994) Tectonic evolution of the emergent part of a volcanic ocean island: Lanzarote, Canary Islands. *Tectonophysics,* **293,** 111-135.

Mercier J.C. (1980) Single-Pyroxene Thermobarometry. *Tectonophysics,* **70**, 1-37.

Morgan, J.P., Morgan, W.J. (1999) Two-stage melting and the geochemical evolution of the mantle: a recipe for mantle plum-pudding. *Earth and Planetary Science Letters,* **170**, 215-239.

Morgan, J.W., Wandless, G.A., Petrie, R.K., Irving, A.J. (1981) Composition of the Earth's upper mantle: I. Siderophile trace elements in ultramafic nodules. *Tectonophysics,* **75**, 47-67.

Morgan W.J. (1972) Deep mantle convection plumes and plate motions, *American Association of Petroleum,* **56**, 203-213.

Morgan, W.J. (1981) Hotspot tracks and the opening of the Atlantic and Indian oceans. In: Emiliani, C. (Ed.) *The Sea*. John Wiley, New York.

Neumann, E.-R. (1991) Ultramafic and mafic xenoliths from Hierro, Canary Islands: Evidence for melt infiltration in the upper mantle. *Contributions to Mineralogy and Petrology,* **106**, 236-252.

Neumann, E.-R., Wulff-Pedersen, E., Johnsen, K., Andersen, T., Krogh, E. (1995) Petrogenesis of spinel harzburgite and dunite suite xenoliths from Lanzarote, eastern Canary Islands: Implications for the upper mantle. *Lithos,* **35**, 83-107.

Neumann E.R., Sorensen V.B., Simonsen S.L., Johnsen K. (2000) Gabbroic xenoliths from La Palma, Tenerife and Lanzarote; evidence for reactions between mafic alkaline Canary Islands melts and old oceanic crust: *Journal of Volcanology and Geothermal Research,* **103**, p. 313-342.

Neumann, E.-R., Wulff-Pedersen, E., Pearson, N.J., Spencer, E.A. (2002) Mantle xenoliths from Tenerife (Canary Islands): Evidence for reactions between mantle peridotites and silicic carbonatite meltings including Ca metasomatism. *Journal of Petrology,* **43**, 825-857.

Neumann, E.-R., Griffin, W.L., Pearson, N.J., O'Reilly, S.Y. (2004) The evolution of the upper mantle beneath the Canary Islands: Information from trace element and Sr isotopic ratios in minerals in mantle xenoliths. *Journal of Petrology,* **45**, 2573-2612.

Neumann, E.-R., Simon, N.S.C. (2009) Ultra-refractory mantle xenoliths from ocean islands: How do they compare to peridotites retrieved from oceanic sub-arc mantle? *Lithos*, **107**, 1-16.

Paris R., Guillou H., Carracedo J.C., Pérez F.J. (2005) Volcanic and morphological evolution of La Gomera (Canary Islands), based on new K/Ar ages and magnetic stratigraphy: implications for oceanic island evolution. *Journal of the Geological Society of London,* **162**, 501-512.

Pearson D.G., Canil D., Shirey S.B. (2003) Mantle Samples Included in Volcanic Rocks: Xenoliths and Diamonds: *Treatise on Geochemistry* **2: The Mantle and Core**, 171-275.

Pearson, D.G., Wittig, N. (2008) Formation of Archean continental lithosphere and its diamonds: The root of the problem. *Journal of the Geological Society*, **165**, 895-914.

Rehkamper M., Halliday A.N. Fitton J.G., Lee. D.C., Wieneke M., Arndt, N.T. (1999) Ir, Ru, Pt, and Pd in basalts and komatiites: new constraints for the geochemical behavior of the platinum-group elements in the mantle. *Geochimica et Cosmochimica Acta,* **63**, 3915-3934.

Ringwood A.E. (1975) Composition and petrology of earth's mantle. New York, McGraw-Hill.

Rudnick R.L., Walker R.J. (2009) Interpreting ages from Re–Os isotopes in peridotites. *Lithos,* **112**, 1083-1095.

Sachs P., Stange S. (1993) Fast assimilation of xenoliths in magmas. *Journal of Geophysical Research,* **98**, 19741-19754.

Sachtleben T., Seck H.A. (1981) Chemical Control of Al-Solubility in Orthopyroxene and its Implications on Pyroxene Geothermometry. *Contributions to Mineralogy and Petrology,* **78**, 157-165.

Schmincke H.U., Klugel A., Hansteen T.H., Hoernle K., Bogaard P. (1998) Samples from oceanic crust beneath Gran Canaria, La Palma and Lanzarote (Canary Islands). *Earth and Planetary Science Letters,* **163**, 343-360.

Schmincke, H.-U., 1982. Volcanic and chemical evolution of the Canary Islands. In: U. von Rad, K. Hinz, M. Sarnthein and E. Seibold (Editors), Geology of the Northwest African Continental Margin. Springer Verlag, New York, N.Y., 273 -306.

Hoernle K., Schmincke H.U. (1993) The role of partial melting in the 15-Ma Geochemical evolution of Gran Canaria: a blob model for the Canary Hotspot. *Journal of Petrology,* **34**, 599-626.

Siena, F., Beccaluva, L., Coltorti, M., Marchesi, S., Morra, V. (1991) Ridge to hot-spot evolution of the Atlantic lithospheric mantle: evidence from Lanzarote peridotite xenoliths (Canary Islands). *Journal of Petrology, Special Lithosphere Issue,* **32**, 271-290.

Simon, N.S.C., Neumann, E.-R., Bonadiman, C., Coltorti, M., Delpech, G., Grégoire, M., Widom, E. (2008) Ultra-refractory domains in the oceanic mantle lithosphere sampled as mantle xenoliths at ocean island. *Journal of Petrology,* **49**, 1223-1251.

Spera F. (1984) Carbon dioxide in petrogenesis III: role of volatiles in the ascent of alkaline magma with special reference to xenolith-bearing mafic lavas. *Contributions to Mineralogy and Petrology,* **88**, 217-232.

Turcotte D.L., Oxburgh ER (1976) Stress accumulation in the lithosphere. *Tectonphysics,* **35**, 183-199.

Turcotte D.L., Schubert G. (1982) Geodynamics Applications of continuum physics to geological problems. Wiley & Sons, Inc. New York.

Widom, E., Hoernle, K.A., Shirey, S.B. & Schmincke, H.-U. (1999) Os isotope systematics in the Canary Islands and Madiera: lithospheric contamination and mantle plume signatures. *Journal of Petrology,* **40**, 279-296.

Workman R.K., Hart S.R. (2005) Major and trace element compositions of the depleted MORB mantle (DMM). *Earth and Planetary Science Letters* **231**, 53-72.

Wulff-Pedersen, E., Neumann, E.-R., Jensen, B.B. (1996) The upper mantle under La Palma, Canary Islands: Formation of Si-K-Na-rich melt and its importance as a metasomatic agent. *Contributions to Mineralogy and Petrology,* **139**, 326-338.